Original Research Article

EVs from cells at the early stages of chondrogenesis delivered by injectable SIS dECM promote cartilage regeneration

Journal of Tissue Engineering
Volume 15: 1–22

DOI: 10.1177/20417314241268189
journals.sagepub.com/home/tej
Sage

Weilai Zhu[1], Jiaying Shi[1], Bowen Weng[1], Zhenger Zhou[1], Xufeng Mao[2], Senhao Pan[1], Jing Peng[1], Chi Zhang[2], Haijiao Mao[2], Mei Li[3] and Jiyuan Zhao[1]

Abstract

Articular cartilage defect therapy is still dissatisfactory in clinic. Direct cell implantation faces challenges, such as tumorigenicity, immunogenicity, and uncontrollability. Extracellular vesicles (EVs) based cell-free therapy becomes a promising alternative approach for cartilage regeneration. Even though, EVs from different cells exhibit heterogeneous characteristics and effects. The aim of the study was to discover the functions of EVs from the cells during chondrogenesis timeline on cartilage regeneration. Here, bone marrow mesenchymal stem cells (BMSCs)-EVs, juvenile chondrocytes-EVs, and adult chondrocytes-EVs were used to represent the EVs at different differentiation stages, and fibroblast-EVs as surrounding signals were also joined to compare. Fibroblasts-EVs showed the worst effect on chondrogenesis. While juvenile chondrocyte-EVs and adult chondrocyte-EVs showed comparable effect on chondrogenic differentiation as BMSCs-EVs, BMSCs-EVs showed the best effect on cell proliferation and migration. Moreover, the amount of EVs secreted from BMSCs were much more than that from chondrocytes. An injectable decellularized extracellular matrix (dECM) hydrogel from small intestinal submucosa (SIS) was fabricated as the EVs delivery platform with natural matrix microenvironment. In a rat model, BMSCs-EVs loaded SIS hydrogel was injected into the articular cartilage defects and significantly enhanced cartilage regeneration in vivo. Furthermore, protein proteomics revealed BMSCs-EVs specifically upregulated multiple metabolic and biosynthetic processes, which might be the potential mechanism. Thus, injectable SIS hydrogel loaded with BMSCs-EVs might be a promising therapeutic way for articular cartilage defect.

Keywords

Cartilage regeneration, extracellular vesicles, chondrogenesis stage, injectable dECM hydrogel, bone mesenchymal stem cells

Date received: 3 May 2024; accepted: 18 July 2024

[1]Zhejiang Key Laboratory of Pathophysiology, School of Medicine, Ningbo University, Ningbo, Zhejiang, People's Republic of China
[2]Department of Orthopaedic Surgery, The First Affiliated Hospital of Ningbo University, Ningbo, Zhejiang, People's Republic of China
[3]Zhejiang Key Laboratory of Precision Medicine for Atherosclerotic Diseases, The First Affiliated Hospital of Ningbo University, Ningbo, Zhejiang, People's Republic of China

Corresponding authors:
Jiyuan Zhao, Zhejiang Key Laboratory of Pathophysiology, School of Medicine, Ningbo University, 818 Fenghua Road, Ningbo, Zhejiang 315211, People's Republic of China.
Email: zhaojiyuan@nbu.edu.cn

Mei Li, Zhejiang Key Laboratory of Precision Medicine for Atherosclerotic Diseases, The First Affiliated Hospital of Ningbo University, 31 Guangji Street, Ningbo, Zhejiang 315201, China.
Email: meili@nbu.edu.cn

Graphical Abstract

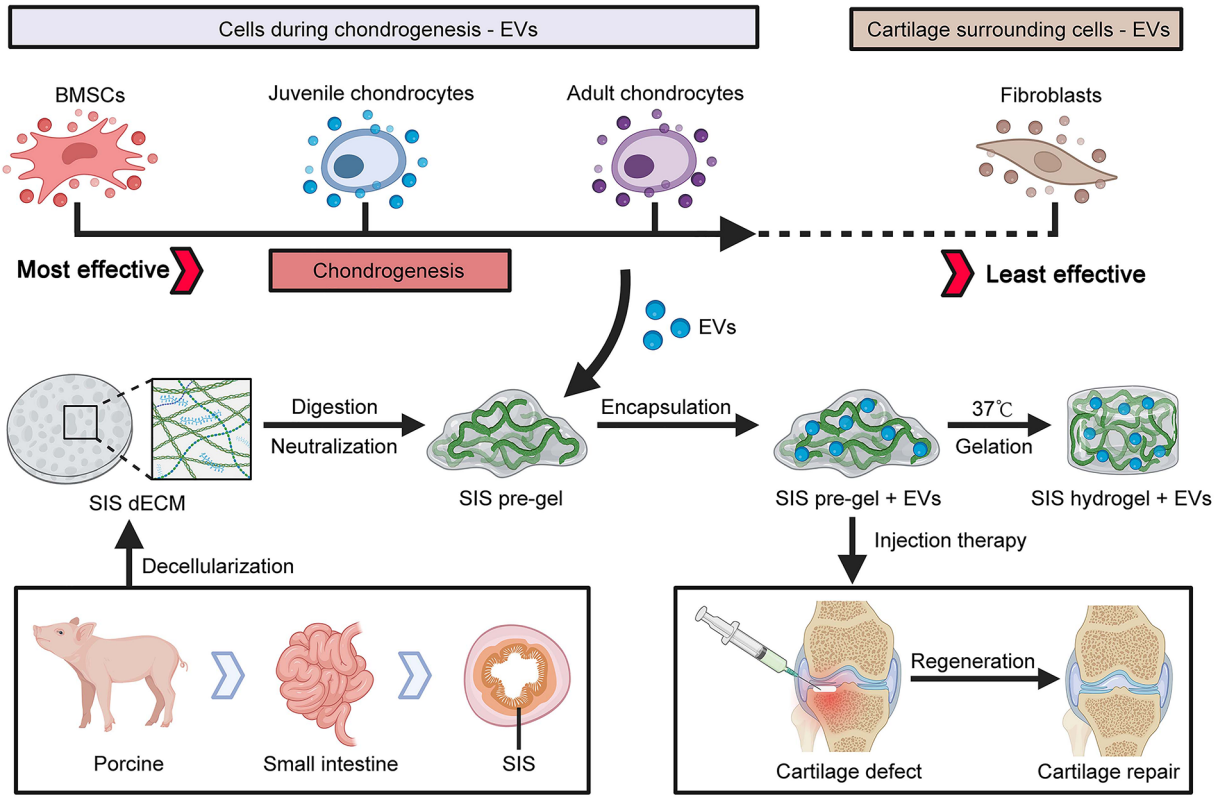

Introduction

Articular cartilage has remarkable load-bearing and low friction properties that maintain smooth movement of joints.[1] The unique cartilage microenvironment lacks vascular, neural, and lymphatic networks leading to limited self-regenerative capacity.[2] Traditional treatments that include surgery and medication are unable to fully heal the injured cartilage to functional hyaline cartilage.[3–5] Tissue engineering offers a promising approach to finding safe and reliable treatments for cartilage defects.

The tissue microenvironment of the articular cartilage injury niche is a crucial factor influencing cartilage remodeling via cell communication and signaling transport.[6] EVs are rich in proteins, enzymes, RNA and DNA. By delivering biological information molecules to recipient cells, EVs can involve in various biological responses.[7–9] EVs-based cell-free therapy is regarded as an ideal alternative to cell therapy to avoid the problems associated with cell implantation while preserving similar functions.[10] Since EVs derived from different tissues have distinctive vesicle contents,[11,12] the effects and action mechanisms vary considerably, suggesting EVs may influence their microenvironment in a tissue source-dependent manner.[13] Lacking a valuable reference, researchers select EVs for cartilage tissue engineering studies usually based on availability and personal preference. Meanwhile, the sluggish regeneration of cartilage emphasizes the limitations of the current EV injection therapy, including low retention and instability.[14] Therefore, suitable sources and effective therapeutic modalities of EVs for cartilage tissue engineering are required.

Chondrocytes and BMSCs are directly involved in the injury microenvironment, and the role of their EVs in cartilage regeneration is of interest.[15,16] Notably, chondrocyte is the final stage of chondrogenic differentiation in BMSCs.[17] BMSCs have the highest self-renewal capacity and differentiation potential, while chondrocytes carry cartilage directional signals and have a strong matrix-producing capacity.[17,18] Kim et al reported that coculture juvenile chondrocytes and adult BMSCs improve their chondrogenesis via EVs but could not see this synergistic effect when adult chondrocytes were cultured with fetal BMSCs, which indicated the communication directionality between chondrocytes and BMSCs may depend on the cell chondrogenesis stage.[19] In the time dimension, within BMSCs-EVs, juvenile chondrocyte-EVs, and adult chondrocytes-EVs, which stage-derived EVs could provide the strongest signal of chondrogenesis to the degenerated chondrocytes and recruited BMSCs in injury situ remain unknown. Meanwhile, fibroblasts directly surround articular cartilage as soft tissues. Our previous study demonstrated

that EVs from fibroblasts as messengers to osteoblasts in a coculture system promoted bone regeneration.[20] Some studies have focused on fibroblasts-EVs for cartilage regeneration,[21] but without comparing them to bone tissue-derived EVs.

The delivery platform of EVs is also essential to the effect on cartilage defect repair. Hydrogels are three-dimensional (3D) scaffolds with a chemically or physically cross-linked structure, they allow the slow release of EVs and achieve long-term effects.[22,23] Recent advances in hydrogels have made decellularized extracellular matrix (dECM) bionic hydrogels a popular scaffold for tissue engineering.[24] Compared with chemosynthetic scaffolds, dECM hydrogels could better mimic the complex components and structure of native microenvironment.[25] Moreover, dECM hydrogels could self-gelation at 37℃ and are suitable for minimally invasive therapy by injection.[26] Small intestinal submucosa (SIS) is a natural collagenous dECM material,[27] collagen also being the main organic component of natural cartilage.[2] SIS with preserved bioactive factors is bioactive and biodegradable, which is FDA-approved for clinical use.[28] Our previous studies have generated and validated multiple SIS dECM scaffolds with potential osteogenic and osteoinductive properties.[20,29–31] Though studies have shown that SIS sheet scaffolds can promote cartilage regeneration,[32] the application of SIS hydrogels in cartilage tissue engineering was rarely reported.

Here, we surmised that combining SIS hydrogel with EVs derived from potential chondrogenesis property cells can promote cartilage repair. We investigated the chondrogenesis stage effect on EVs chondrogenesis capability, and fibroblast-EVs was also joined to compare. Fibroblasts, juvenile chondrocytes, adult chondrocytes, and BMSCs were expanded to obtain their corresponding EVs. Their potential effects on the viability, migration, and chondrogenic differentiation of chondrocytes and BMSCs were evaluated. Meanwhile, we successfully fabricated injectable SIS hydrogel and investigated the cartilage regeneration ability of different EVs in vivo based on the SIS hydrogel delivery platform. Moreover, the proteomic characteristics of different EVs were explored to investigate the potential mechanisms of their different bioactivities.

Materials and methods

Ethic statement

All experimental procedures involving animals were conducted in compliance with Chinese legislation regarding the use and care of laboratory animals and were ethically approved by the Animal Care and Use Committee of Ningbo University. The approved protocol number is NBU20220091. All experimental animals were purchased from Charles River (Zhejiang, China) and housed under specific pathogen-free conditions in the Animal Center of Ningbo University.

Isolation of BMSCs and cell culture

Wistar rats (2 week, male) were terminated by cervical dislocation. Muscles, ligaments, and tendons were carefully disassociated from the tibias, femurs, and humeri. The marrow is slowly flushed out using a syringe with culture medium until the bones become pale and then incubated at 37℃, 5% CO_2 for 5 days. After BMSCs were adherent to the culture dish surface, changing the medium to remove nonadherent cells.[33] The culture medium was changed every 2 days. The cells were passaged upon reaching 80% confluence. To ensure cell viability, this experiment only used cells from passage 3 to passage 4.

NIH/3T3 cells were obtained from the Cell Bank of the Chinese Academy of Sciences (Shanghai, China). C20A4 cells (juvenile chondrocyte) and C28I2 cells (adult chondrocyte) were obtained from BLUEFBIO™ (Shanghai, China). All cells were cultured in DMEM supplemented with 10% fetal bovine serum (FBS), penicillin (100 U/mL)-streptomycin (0.1 mg/mL). For NIH/3T3 cells, an additional 0.1 mM NEAA (non-essential amino acid) was provided. Chondrogenic induction medium for BMSCs consisting of the DMEM supplemented with 1% (v/v) Insulin-Transferrin-Selenium-A (Gibco), 0.1 μM dexamethasone (Sigma), 50 μg/mL ascorbic acid-2-phosphate (Shyuanye), and 10 ng/mL TGF-B3 (Peprotech).

Isolation and characterization of EVs

FBS was previously ultracentrifuged at 100,000 g for 8 h to remove exogenous EVs. NIH/3T3, C20A4, C28I2, and BMSCs cells were seeded in culture medium. When cells reached 60% confluence, the FBS in the culture medium was replaced with EV-depleted FBS for 48 h prior to the collection of the conditioned medium (CM). Firstly, the CM was centrifuged at 300 g (10 min), 2000 g (30 min), and 12,000 g (30 min) in turn, followed by filtration using a 0.22 μm filter (Merck Millipore, Burlington, MA) to remove the remaining cells and debris. Then, after ultracentrifugation at 100,000 g for 90 min, the raw EVs extract was washed with phosphate-buffered saline (PBS) once. Followed by another ultracentrifugation at 100,000 g for 90 min, the pure EVs were resuspended with PBS and stored at −80℃. All the above centrifugal processes were carried out at 4℃.

Transmission electron microscopy (TEM, HT7800, Hitachi, Japan) and dynamic light scattering system (DLS, Zetasizer Nano ZS, Malvern, UK) were used to observe EVs morphology and size distribution. The BCA Protein Quantitative Kit (Transgene) was used to confirm the protein concentrations of EVs. The EVs characteristic protein markers, including TSG101 (A2216, ABclonal, Shanghai,

Table 1. Primer sequences for real-time qPCR amplification.

Genes	Species	Primer sequences (5'–3')	Length (bps)
SOX9	Human	F: GGCAAGCTCTGGAGACTTCTG R: CCCGTTCTTCACCGACTTCC	138
Sox9	Rat	F: AGTCGGTGAAGAATGGGCAA R: CTGAGATTGCCCGGAGTGC	158
COL2A1	Human	F: TGGACGATCAGGCGAAACC R: GCTGCGGATGCTCTCAATCT	244
Col2a1	Rat	F: CCCCTGCAGTACATGCGG R: CTCGACGTCATGCTGTCTCAAG	60
ACAN	Human	F: CAGTGCGATGCAGGCTGGCT R: CCTCCGGCACTCGTTGGCTG	234
Acan	Rat	F: CCCAAACAGCAGAAACAGCC R: TCACATTGCTCCTGGTCTGC	106
GAPDH	Human	F: GGTGGTCTCCTCTGACTTCAACA R: GTTGCTGTAGCCAAATTCGTTGT	127
β-*Actin*	Rat	F: AGATGTGGATCAGCAAGCAG R: GCGCAAGTTAGGTTTTGTCA	125

China), CD63(A19023, ABclonal), and CD81(A5270, ABclonal) were detected by Western blot.

EVs labeling and uptake

EVs were labeled with PKH 26(UR52302, Umibio, Shanghai, China) according to the manufacturer's instructions. Briefly, 100 μg EVs were incubated with 50 μL PKH26 reaction mixture for 15 min at room temperature. PKH26 tends to self-aggregate and form micelles that can resemble EVs owing to the amphipathic property.[34] We used a uniform lower concentration level of PKH26 (2μM) which self-assembly occurs less according to the research.[35] After 15 min, a 4950 μL culture medium was added to the EVs-PKH26 solution to stop the staining reaction of PKH26 and adjust the concentration of EVs at 20 μg/mL. To detect the effects of residual dyes on the staining of cell membranes and cell behavior, we set up a control solution for the blank group, 50 μL PKH26 incubated alone for 15 min and then added 4950 μL medium for dilution. PKH26-labeled EVs were added to chondrocytes and BMSCs at a concentration of 20 μg/mL for 12 h. Then used confocal laser microscopy (TCS SP8, Leica, Germany) to determine the uptake of the labeled EVs. DAPI was used to show the nuclei and phalloidin was used to stain F-actin to show the cytoskeleton.

Effect of EVs on cell proliferation, differentiation and migration

For cell proliferation assay. Chondrocytes or BMSCs were seeded at 1000 cells/well on 96-well plates and treated with 20 μg/mL (NIH/3T3, C20A4, C28I2, and BMSCs) EVs or PBS (control). Cell number was determined at 1, 3, 5, and 7 days using a cell counting kit (CCK, TransGen, Beijing, China) following the manufacturer's instructions. Briefly, fresh medium (100 μL) containing CCK reagent (10 μL) was added to each well and incubated at 37℃ for 2 h. The absorbance of the reaction medium at 450 nm was then measured using a microplate reader.

For cell differentiation ability assay. After being treated with 20 μg/mL (NIH/3T3, C20A4, C28I2, and BMSCs) EVs or PBS for 3 and 7 days, the total mRNA was isolated from chondrocytes or BMSCs cultures using RNA-Solv reagent (Omega Engineering, Inc., Norwalk, CT). RNA concentration and purity were then measured by a microplate spectrophotometer at 230, 260, and 280 nm UV absorbance. TransStart® One-Step gDNA Removal and cDNA Synthesis SuperMix (AT311, TransGen) were used to reverse transcript mRNA into cDNA. Real-time q-PCR was performed with TransStart® Top Green qPCR SuperMix (P41014, TransGen). GAPDH and β-actin were used as endogenous control. The primer sequences are shown in Table 1.

For wound healing assay. Chondrocytes or BMSCs were seeded on 12-well plates as a monolayer. After cells were starved in 3% FBS medium for 12 h, a 200-μL pipette tip was used to scratch the cell surface with a straight line. Subsequently, washed the dropped cells with PBS. Then treated the cells with four kinds of 20 μg/mL EVs or PBS. Scratch area healing images were obtained and calculated at indicated times.

Generation of EVs-SIS hydrogel

The small intestine was harvested from healthy home-raised pigs within 4 h of sacrifice. Remove the tunica serosa and tunica muscularis by mechanical delamination to isolate the original SIS. After overnight wash, SIS was treated for decellularized with the following solutions

under constant agitation on a shaker: Methanol-chloroform mixture (1:1 volume ratio) for 12 h twice, 0.05% trypsin-0.05%EDTA for 12 h, 0.5% SDS-0.9% NaCl for 4 h and PBS washed 3 times (10 min/time) during each different solution. The decellularized SIS was soaked in 75% ethanol for 20 min and washed 3 times with ddH_2O (10 min/time) to remove the remaining SDS. After freeze-drying for 6 h, dSIS was milled into powder and digested with pepsin/HCl solution (1 mg/mL in 0.1 M HCl) at RT for 72 h. The digestive solution was then centrifuged at 300 g for 5 min to discard undigested particles. Adding 0.1 M NaOH to the digestive solution to neutralize to pH 7.4, adding 10% 10X PBS to equilibrate cytocompatibility salinity, and adding 1 × PBS to adjust the concentration. Finally, the neutralized solution (pre-gel) was incubated at 37℃ for 40 min to gelation (SIS hydrogel).

While on ice and immediately prior to use, the pre-gel solution was homogeneously mixed with the pure EVs extract resuspended in PBS. In this experiment, all EVs-SIS pre-gel was finally adjusted to a concentration of 8 mg/mL for SIS and a concentration of 100 μg/mL for EVs. Gelation took place in 30 min in the incubator.

Decellularization quantification of SIS dECM

Randomly selected original SIS and dSIS were used for the quantification of DNA ($n=5$) and ECM ($n=3$). Residual DNA content was determined by a CyQUANT® cell proliferation kit (C7026, Invitrogen, Shanghai, China) according to the manufacturer's instructions. Total collagen content was indirectly quantified based on the hydroxyproline ratio to collagen (1:7.2 mass ratio) using a Hyp content determination kit (BC0250, Solarbio, Beijing, China). The glycosaminoglycans (GAG) content in SIS and dSIS was determined using a DMMB GAG quantification kit (CM51023.1, GENMED scientifics Inc., Wilmington DE).

Characterization of SIS hydrogel

Scanning electron microscope (SEM) was used to observe the cross-sections of SIS hydrogels. Hydrogels were fixed with 2%formaldehyde-2.5%glutaraldehyde fixative (Solarbio) for 12 h. After ddH_2O washing, samples were dehydrated in 50%, 70%, 90%, 95%, and 100% ethanol for 30 min each, and finally soaked in anhydrous ethanol overnight. The samples were dried using a critical point drier (EM CPD300, Leica, Germany) by circularly entering CO_2 for 4 h. For SEM scanning, the samples were sputter-coated with platinum and viewed using an SEM (SU-70, Hitachi, Japan).

The turbidity of SIS hydrogels for gelation kinetics evaluation was determined by spectrophotometry. For each concentration, 200 μL/well SIS pre-gels were pipetted into a 96-well plate and absorbance at 450 nm was measured every 2 min for 1 h at 37℃. The readings were then normalized to a PBS control and scaled according to the equation below, where NA is the normalized absorbance, A is the absorbance at a given time, Amin is the smallest absorbance, and Amax is the maximum absorbance.

$$NA = \frac{A - Amin}{Amax - Amin}$$

The rheological characteristics of SIS hydrogels were determined with a rotational rheometer (HAAKE™ MARS™ iQ AIR, Thermo Fisher, Germany). 500 μL SIS pre-gels were placed in between the test plates with a gap of 1 mm, and preheated at 25℃. In the oscillation mode of the rheometer, with a frequency of 1 Hz and a strain amplitude of 10%, the temperature was ramped from 25 to 37℃ for 6 min, constant at 37℃ for 30 min, and finally ramped from 37 to 50℃ for 6.5 min. G' and G" were measured for the duration (42.5 min).

Effect of SIS hydrogel on cell growth and proliferation

Direct cell culture on SIS hydrogel surface. Chondrocytes or BMSCs (5×10^3) were cultured on the surface of hydrogels in 96-well plates. After coculture with each concentration of hydrogel for 1, 4, 7, and 14 days, the cell-hydrogel complexes were stained with DAPI and FITC- phalloidin and then observed using a confocal laser microscope (TCS SP8, Leica).

Indirect cell culture with SIS hydrogel using transwell system. Chondrocytes or BMSCs (1×10^4) were seeded on 24-well plates. Transwell upper chambers were covered with 200 μL 8 mg/mL SIS hydrogel, placed on the cell cultured plate, and soaked in the culture medium. CCK reagent was performed to detect cell viability in the lower chamber at 1, 3, 5, and 7 days as mentioned above.

Effect of EVs-SIS hydrogel on cell migration

Cell migration from media to SIS hydrogel was assessed using a 24-well plates transwell system. 20 μL 8 mg/mL SIS hydrogel was ornamented on the underside of the transwell membrane. Chondrocytes or BMSCs (3×10^4) were seeded on the upside of the membrane in the upper chamber. To determine the chemotactic response of chondrocytes or BMSCs with EVs-SIS hydrogels, transwell upper chamber was seeded with chondrocytes or BMSCs (2×10^4) and the lower chamber was covered with 300 μL 8 mg/mL SIS hydrogel containing 100 ug/mL four kinds of EVs or equal volume PBS. The upper chamber was filled with 5% FBS media in two assays, and the lower chamber was filled with 20% FBS media. After 12 h incubation,

cells remaining at the upside of the membrane were wiped with a cotton swab, and the cells on the underside of the membrane were fixed and stained with 0.5% crystal violet solution. Membranes were observed and calculated under an inverted microscope. Cell counting was calculated by ImageJ software (National Institutes of Health, USA).

Rat articular cartilage defect model

Following the previously published method,[36] a total of 15 healthy male Sprague-Dawley(SD) rats of 8 weeks were involved in the experiment. Two knee joints per rat, thirty knee joints in total, *n* represents the number of knee joints. Each knee joint formed one defect individually, and two knees of one rat were implanted with different materials to avoid individual differences. The thirty knee joints were divided into six groups: (I) Blank (PBS) group ($n=5$); (II) SIS hydrogel group ($n=5$); (III) SIS + NIH/3T3-EVs group ($n=5$); (IV) SIS + C20A4-EVs group ($n=5$); (V) SIS + C28I2-EVs group ($n=5$); (VI) SIS + BMSCs-EVs group ($n=5$). Rats were anesthetized with 3% sodium pentobarbital (1%, 100 mg/kg) by intraperitoneal injection. A lateral parapatellar longitudinal incision was created to reveal the knee joint. After synovial capsule incision and medial patella luxation, the trochlear groove was exposed. An osteochondral defect (2 mm in diameter and 1.5 mm in depth) was created with Kirschner wire in the center of the trochlear groove. Different implants were injected to fill the defects according to the above groupings. The concentration of SIS hydrogel was 8 mg/mL. The concentration of EVs was 100 ug/mL. The rats were sacrificed at 10 weeks after the operation, and the knee joints were surgically collected and fixed in 4% formaldehyde for further testing.

Histological staining and analysis

The fixed specimens were rinsed with PBS, decalcified, dehydrated, embedded in paraffin, and sectioned for staining. Hematoxylin and eosin (HE) staining, toluidine blue (TB) staining, and Safranin-O (Saf-O) staining were conducted according to the manufacturer's instructions of staining kit (Solarbio). Images of histological sections from the lateral and medial regions of each defect (five images per specimen) were captured using a digital camera. The quality of cartilage repair was assessed by calculating the new-formed cartilage area and using the Wakitani scoring system by blinded independent researchers.

Immunofluorescence (IF) and immunohistochemical (IHC) staining

Sections were subjected to IF and IHC staining to visualize protein distribution patterns and protein expression levels. COL II (A1560, ABclonal) and COL I (ab21286, Abcam) primary antibodies, and secondary antibodies conjugated with Alexa Fluor® 555 (CST, Shanghai, China) were applied for IF. DAPI was used to show nuclei. The immunohistochemical staining was conducted using the DAB (ab161117, Abcam, Shanghai, China) staining method. Aggrecan primary antibodies (A8536, ABclonal) were used for IHC.

Proteomic analysis of EVs

Protein identification by 4D label-free technology could reveal four kinds of EVs relative protein expression levels. Freshly purified EVs samples were incubated with SDT lysis buffer (4% SDS, 100 mM DTT, 150 mM Tris-HCl pH 7.6). The proteins were then undergoing tryptic digestion process following the filter-aided sample preparation (FASP) protocol.[37] The peptides were solubilized in buffer A (0.1% Formic acid) and separated with a linear gradient of buffer B (84% acetonitrile and 0.1% Formic acid) using a Nanoelute (Bruker Daltonics, Bremen, Germany). Liquid crystal tandem mass spectrometry (LC-MS/MS) analysis was performed on a timsTOF Pro mass spectrometer (Bruker Daltonics) in positive ion mode with a primary mass spectrum acquisition and 10 cycles of PASEF (Parallel cumulative serial fragmentation) MS/MS. The MS data were searched by MaxQuant v. 1.6.14. Normalization (−1, 1) of the examined protein relative expression data was used to perform hierarchical clustering analysis. The protein sequences were retrieved from Universal Protein (UniProt). Significantly differential proteins were subjected to Gene Ontology (GO) and Kyoto Encyclopedia of Genes and Genomes (KEGG) analyses.

Statistical analysis

All quantitative data were expressed as the means ± standard deviation (SD). Statistical analyses were performed using SPSS® software (Chicago, IL). For multiple comparisons, statistical significance was determined using one-way analysis of variance (ANOVA) followed by a post hoc test (Bonferroni). For the comparison of the two groups, student t-test was used for calculation. $*p<0.05$ was considered statistically significant.

Results

Characterization and uptake of EVs

NIH/3T3-EVs, C20A4-EVs, C28I2-EVs, and BMSCs-EVs extracts were collected respectively. They were then characterized to ensure that the extracts obtained are of EVs and to identify potential differences in physicochemical properties. TEM observations showed that all the four types of samples appeared as typical disc vesicles with complete cell membrane structure (Figure 1(a)). Data from

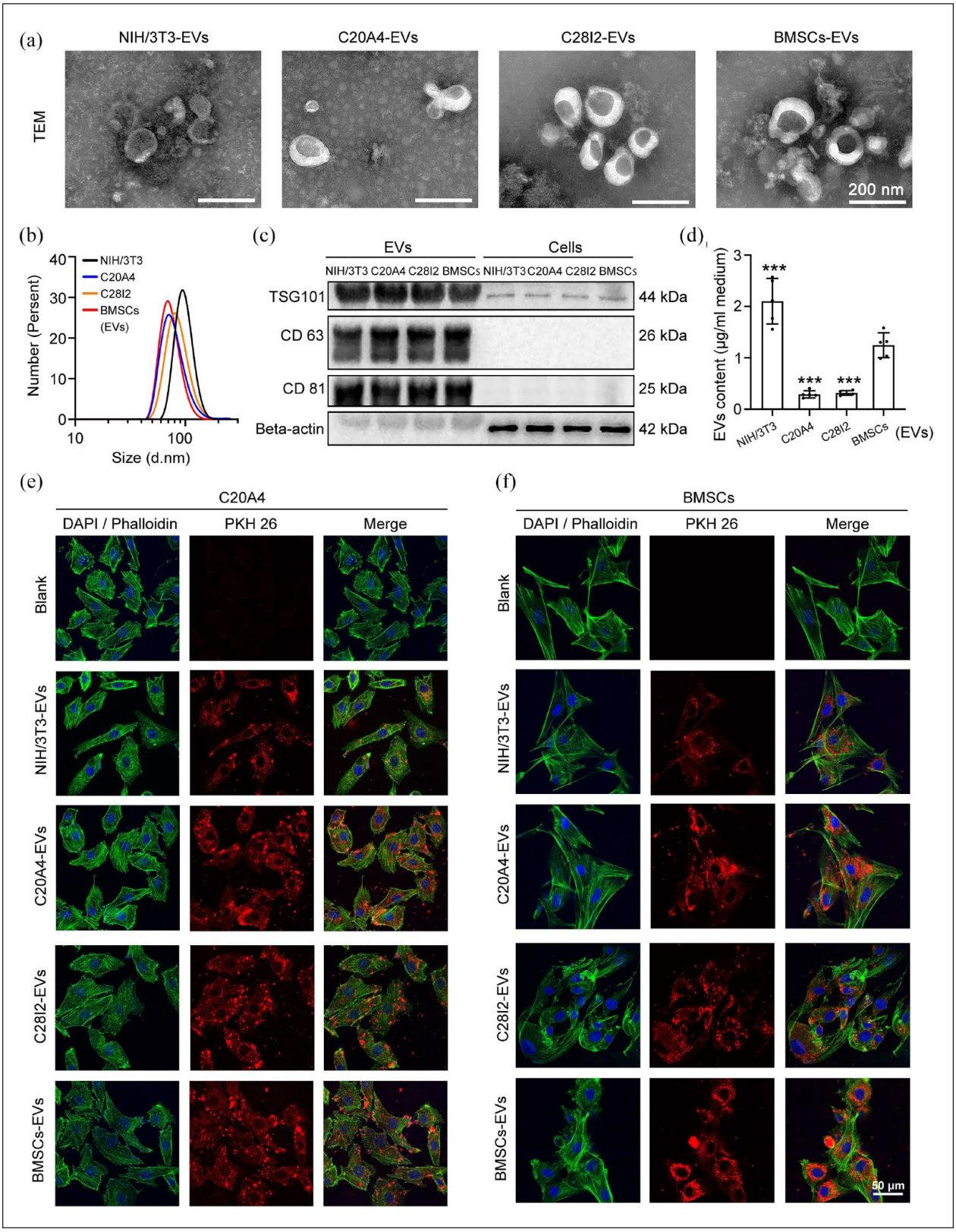

Figure 1. Characterization and uptake of EVs: (a) TEM images of EVs from fibroblasts, juvenile chondrocytes, adult chondrocytes, and BMSCs (NIH/3T3-EVs, C20A4-EVs, C28I2-EVs, and BMSCs-EVs), (b) particle size distribution of EVs measured by DLS, (c) western blot analysis for EVs and cellular markers, (d) EV yields from conditioned medium (*$p < 0.05$. **$p < 0.01$. ***$p < 0.001$. $n = 5$), (e) confocal microscopy demonstrated the uptake of PKH26-labeled EVs (red) by C20A4 cells and BMSCs in vitro.

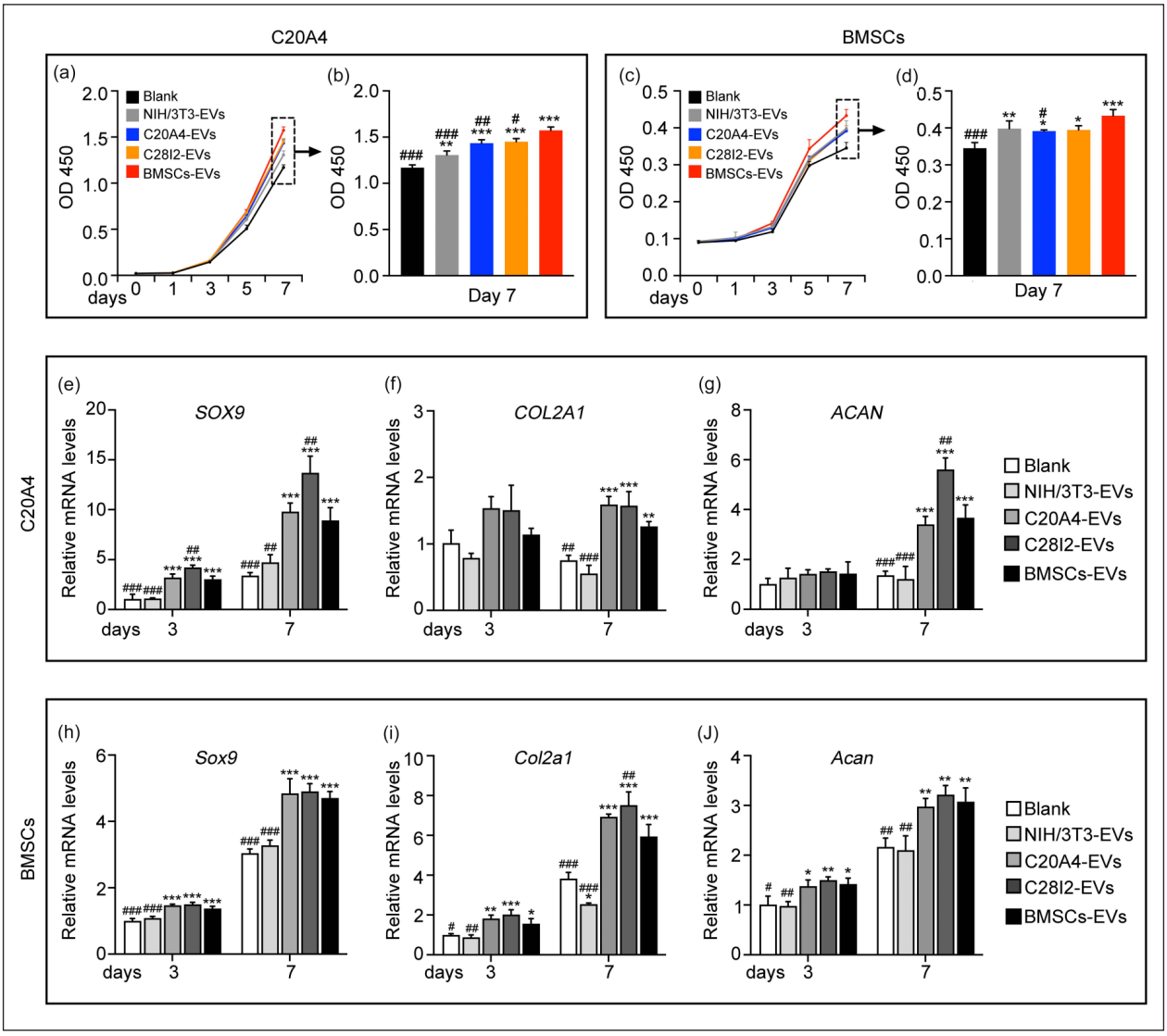

Figure 2. Cell proliferation and chondrogenic differentiation assessment of chondrocytes and BMSCs treated with EVs from different origins. Effects of EVs on the proliferation of C20A4 cells (a–b) and BMSCs (c–d) (CCK-8 method). The relative gene expression levels of the chondrogenic genes (*SOX9, COL2A1, ACAN*) in C20A4 cells (e–g) and BMSCs (h–j).
*Compared with blank group. #Compared with BMSCs-EVs group. */#$p < 0.05$. **/##$p < 0.01$. ***/###$p < 0.001$. $n = 3$.

DLS revealed that four types of EVs had a similar distribution of particle size within 200 nm diameter. The main diameter peaks were in the range of 60–100 nm (Figure 1(b)), which was in accordance with the TEM results. In addition, western blot analysis revealed that the classical EVs-specific markers TSG101, CD63, and CD81 highly enriched while beta-actin was lowly expressed in EVs lysates, compared to whole-cell lysates (Figure 1(c)). After the same centrifugation steps with conditioned media from different cells, protein quantification by BCA assay revealed more EVs extracts from fibroblasts and BMSCs conditioned media (Figure 1(d)). This implied that fibroblasts and BMSCs secrete more EVs.

To confirm the role of EVs on cells, PKH-26 was used to label EVs. Figure 1(e, f) showed the presence of PKH26-labeled EVs in the cytoplasm of the cells and distributed around the nucleus, indicating that EVs were successfully internalized by chondrocytes or BMSCs, and further affected the cell behaviors. Interestingly, C20A4-EVs, C28I2s-EVs, and BMSCs-EVs treated groups seemed to have a stronger signal than NIH/3T3-EVs treated group, which was consistent in both chondrocytes (Figure 1(e)) and BMSCs (Figure 1(f)).

Effect of different EVs on cell behaviors

Chondrocytes and BMSCs proliferation, differentiation, and migration are fundamental properties for in vivo cartilage tissue reconstruction. CCK-8 tests showed a considerable upregulation of proliferation rate with four types of

EVs treatments (20 μg/mL) compared with the blank (PBS), while BMSCs-EVs showed the major effect both on chondrocytes and BMSCs (Figure 2(a–d)). By 7 days, the proliferation of chondrocytes with BMSCs-EVs treated significantly increased compared to other groups (Figure 2(b)). Similarly, BMSCs-EVs were more efficient for BMSCs proliferation (Figure 2(d)).

qRT-PCR assay was used to determine the effect of EVs on chondrogenic differentiation. For both chondrocytes and BMSCs, the expression of the hyaline cartilage-specific genes SRY-box transcription factor 9 (*SOX9*), collagen type II alpha 1 (*COL2A1*) and aggrecan (*ACAN*) in the groups were significantly upregulated after 7 days of induction compared to the blank group, with the most increment in the C28I2-EVs group (Figure 2(e–j)). The C20A4-EVs had similar differentiation effects to BMSCs-EVs. However, the NIH/3T3-EVs treated group had no significant increase in the expression compared to the blank group. This result indicates that EVs with different sources are not equivalent in their capabilities to regulate the chondrogenic differentiation, while C20A4-EVs, C28I2-EVs, and BMSCs-EVs could enhance the chondrogenic differentiation of chondrocytes and BMSCs.

Additionally, we sought to elucidate the migration ability of chondrocytes and BMSCs with EVs treatment by wound healing assay. Compared with the blank group, four EVs-treated groups significantly enhanced wound closure. In detail, the enhancement of cell migration in the BMSCs-EVs, C28I2s-EVs, C20A4-EVs, and NIH/3T3-EVs -treated chondrocytes decreased in sequence (Figure 3(a, c)). For BMSCs, BMSCs-EVs, and NIH/3T3-EVs had a stronger capacity to facilitate migration relative to two chondrocyte-EVs groups (Figure 3(b, d)). Interestingly, BMSCs-EVs treated group had the highest extent of wound closure observed in both chondrocytes and BMSCs.

Generation and characterization of SIS hydrogels

Hydrogels were successfully fabricated from the original SIS at a concentration ranging from 4 to 12 mg/mL through the processing steps in Figure 4(a) and were found to be injectable through a syringe and 18 G needle. The DNA content of SIS was significantly decreased after decellularization, confirmed the current trypsin-SDS decellularization protocol can effectively remove the cellular components (Figure 4(b)). Meanwhile, the collagen of dSIS was enriched (Figure 4(c)) and the GAG was not significantly reduced (Figure 4(d)), which confirmed relevant ECM components were successfully preserved in dSIS. Macroscopically, the higher SIS concentration (8–12 mg/mL) hydrogels had a more rigid appearance structure with well-defined edges, while 4–6 mg/mL hydrogels became relatively soft with rounded edges and could not be handled with forceps (Figure 4(e)). SEM morphology of the hydrogel cross-section revealed the internal network detail. Collagen bundles are interwoven in a randomly oriented fibrillar structure, and the fiber pore size decreases with higher SIS concentration (Figure 4(f)).

We evaluated the turbidimetric gelation kinetics of SIS hydrogels by spectrophotometry (Figure 4(g)) and quantified the gelation parameters. For each analyzed concentration (4, 6, 8, 10, 12 mg/mL), NA formed a sigmoidal curve with time, indicating the gelation of SIS pre-gel at 37°C. The formation began after the *T* lag period, and all the analyzed pre-gels concentrations reached 90% gelation within 30 min, while higher concentrations occurred more quickly with lower *T* lag time.

The rheological and mechanical properties of SIS hydrogels are much relevant to cell viability and filling stability.[25] When exposed to 37℃, all concentrations of SIS hydrogels exhibited gel-like properties with higher energy storage modulus (G') than loss modulus (G"). Consistent with rheology, higher concentration gel forms faster. At approximately 45℃, all hydrogels showed a drop in their G', indicating the melting point. The final steady state G' and G" at 37℃ equilibrium of fully formed SIS hydrogels increased non-linearly with concentration. The G" of 8 mg/mL hydrogel was substantially higher than 4 and 6 mg/mL concentrations, but the difference between 8, 10, and 12 mg/mL concentrations was not significant (Figure 4(h, i)).

SIS hydrogel biocompatibility in vitro

The confocal laser observation of cells seeded on the surface of SIS hydrogel (Figure 5(a, b)) showed cells spread out after adherent by the first day then aggregated into clusters and connected into sheets by the seventh day. These results confirmed that SIS hydrogel has good adhesion capability and cytocompatibility. Further, cells gradually infiltrated deeper layers of the hydrogel from the surface. In the 4 mg/mL hydrogel group, the penetration depth of chondrocytes was approximately 120 μm by day 14, which is significantly higher than the 100 and 70 μm observed respectively in the 8 and 12 mg/mL groups during the identical co-culture period. Similarly, the low-concentration gel group was more conducive for BMSCs infiltration, reaching 400 and 300 μm depth respectively in the 4 and 8 mg/mL SIS hydrogel groups on day 14. Combining gelation time, mechanical properties, and biocompatibility, we selected the 8 mg/mL SIS hydrogel with superior performance in all aspects for subsequent experiments.

CCK-8 assay showed a persistent increase in cell viability of chondrocytes and BMSCs in both blank group and 8 mg/mL SIS hydrogel group. The co-culture with hydrogel significantly promoted cell proliferation from day 1 to day 7 (Figure 5(c–e)). Indicating that SIS hydrogel had outstanding biological activity for chondrocytes and BMSCs proliferation.

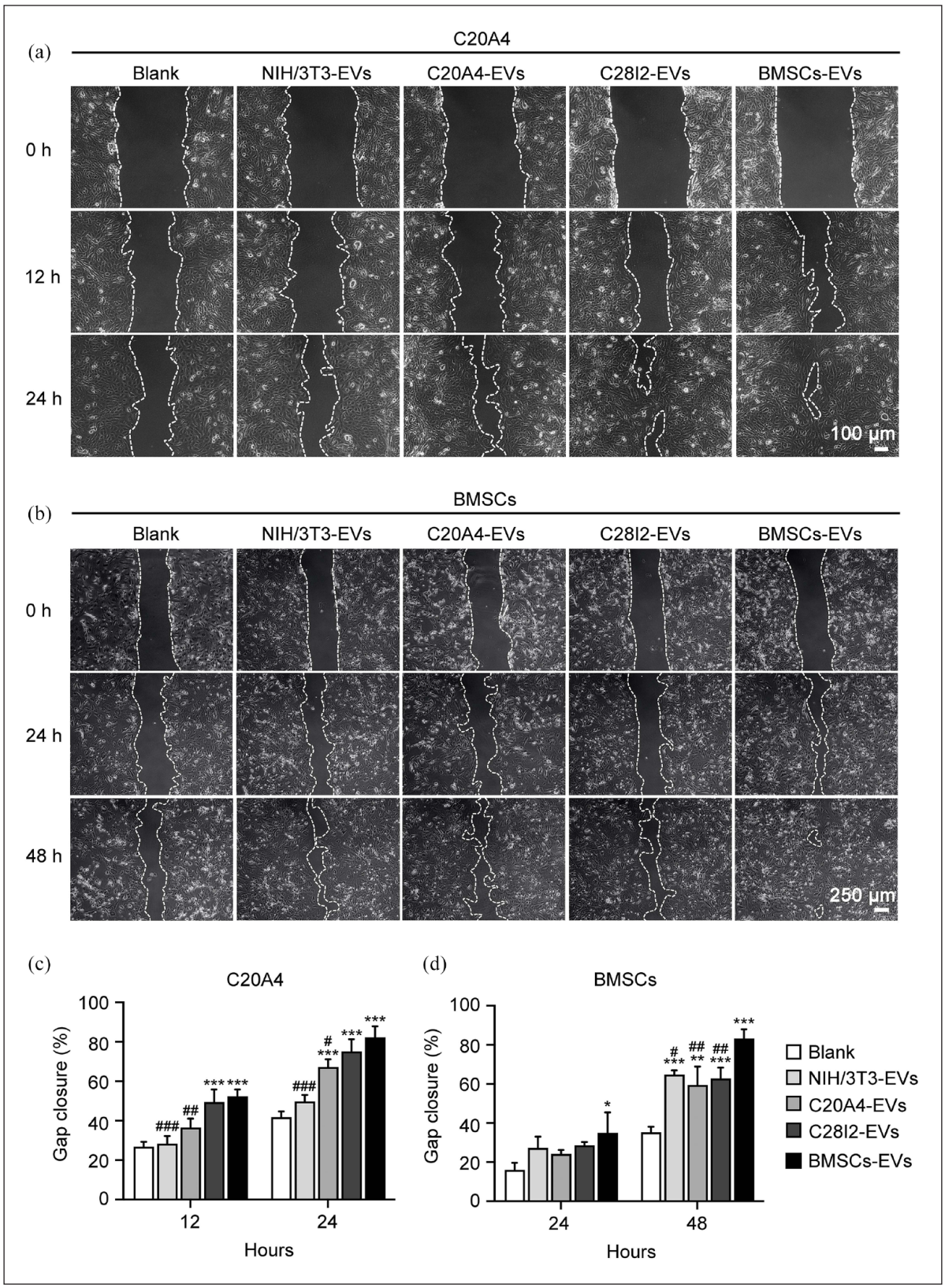

Figure 3. Cell migration assessment of chondrocytes and BMSCs treated with EVs from different origins: (a–b) representative images of wound healing at different time points in C20A4 cells (a) and BMSCs (b), (c–d) quantified percentage of wound closure in C20A4 cells (c) and BMSCs (d).
*Compared with blank group. #Compared with BMSCs-EVs group. $^{*/\#}p < 0.05$. $^{**/\#\#}p < 0.01$. $^{***/\#\#\#}p < 0.001$. $n = 3$.

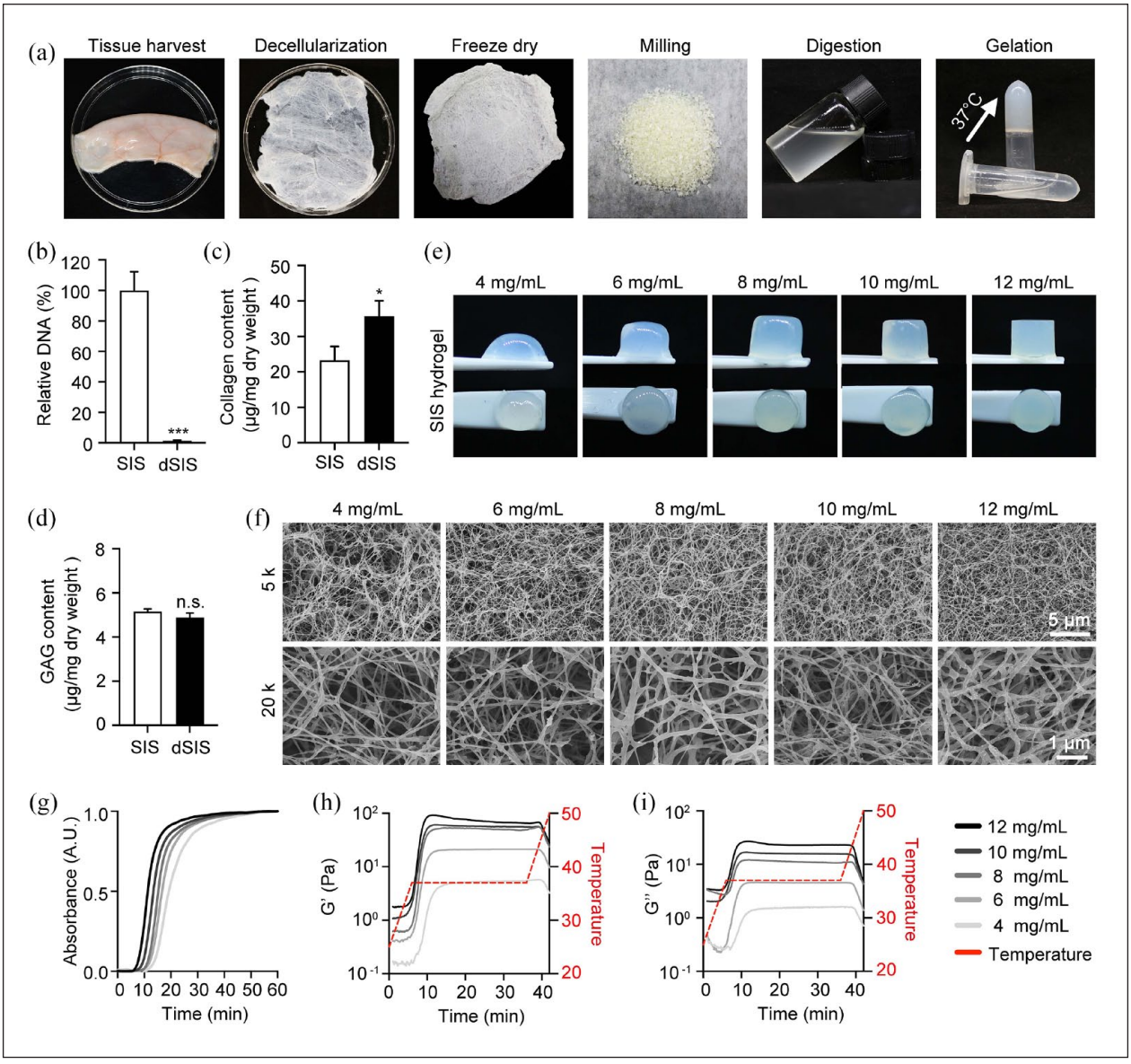

Figure 4. SIS hydrogel characterization: (a) schematic representation of the SIS hydrogel preparation protocol, (b) quantification of residual DNA in original SIS and dSIS. The relative DNA was defined as the percentage of DNA content of dSIS in that of native cells before decellularization ($n = 5$), (c) quantification of collagen content in original SIS and dSIS ($n = 3$), (d) quantification of GAG content in original SIS and dSIS ($n = 3$), (e) macroscopic appearance of hydrogels at different SIS concentrations (4, 6, 8, 10, 12 mg/mL), (f) SEM results for the cross-section of SIS hydrogels displayed the interconnected fibrous network, (g) the turbidimetric gelation kinetics of the SIS hydrogels assessed by spectrophotometry ($n = 3$), (h–i) rheological characterization of SIS hydrogels for both storage modulus (h) and loss modulus (i).
*$p < 0.05$. **$p < 0.01$. ***$p < 0.001$.

The transwell assay results revealed that the migrated chondrocyte number infiltrated in the 8 mg/mL SIS hydrogel was significantly increased compared to the blank group (Figure 5(g, i)). This effect was enhanced for BMSCs. The number of lower chamber BMSCs in the SIS hydrogel groups was nearly eight times that of the blank group (Figure 5(h, j)).

EVs-SIS hydrogel facilitated the chemotactic response of chondrocytes and BMSCs

Another transwell assay was performed to verify that SIS hydrogel could successfully release EVs and investigate the chemotactic effect of hydrogel containing four different cells derived EVs on chondrocytes and BMSCs. In line

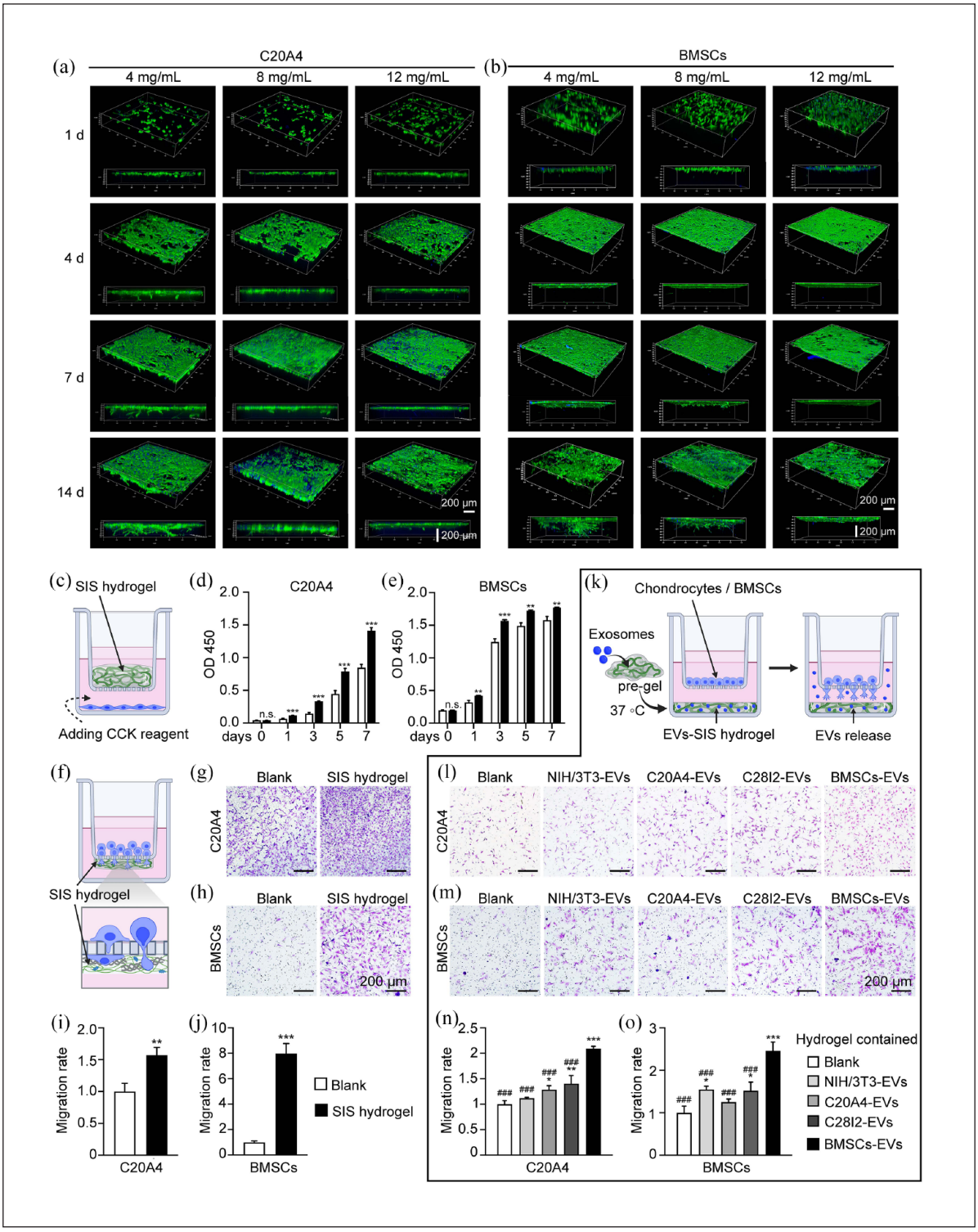

Figure 5. In vitro biological properties of SIS hydrogel and chemotactic effect of EVs-SIS hydrogel: (a–b) confocal laser observation of C20A4 cells (a) and BMSCs (b) planted on the SIS hydrogel for 1, 4, 7, and 14 days, (c–e) effect of SIS hydrogel on cell proliferation, (c) schematic illustration of CCK-8 assay. SIS hydrogel promoted C20A4 cells (d) and BMSCc (e) proliferation, (f–j) effect of SIS hydrogel on cell migration, (f) schematic illustration of transwell migration assay under the conditions of ornamented SIS hydrogel on the underside of the transwell membrane. Representative images of C20A4 cells (g) and BMSCs (h) migrated to the underside of the membrane. Quantified percentage of migration (C20A4 cells (i), BMSCs(j)), (k–o) effect of EVs-SIS hydrogel on cell chemotactic response, (k) schematic illustration of cell chemotactic response assessed by transwell system. Representative images of C20A4 cells (l) and BMSCs (m) from the transwell assay and quantification of the data (C20A4 cells (n), BMSCs (o)).
*Compared with blank group. #Compared with BMSCs-EVs group. $^{*/\#}p < 0.05$. $^{**/\#\#}p < 0.01$. $^{***/\#\#\#}p < 0.001$. $n = 3$.

with the previous wound healing assay results, we observed a significantly higher chemotactic response of chondrocyte in the BMSCs-EVs hydrogel group, followed by the C28I2-EVs hydrogel group, C20A4-EVs hydrogel group, NIH/3T3-EVs hydrogel group and EVs-free hydrogel group (blank group) in sequence (Figure 5(l, n)). For BMSCs, the chemotactic effect of the BMSCs-EVs hydrogel group was evidently the strongest. Unlike chondrocytes, BMSCs appear to have a more notable chemotactic response to fibroblast-EVs than chondrocyte-EVs (Figure 5(m, o)). These results demonstrated that EVs could be released from 8 mg/mL SIS hydrogel, and stimulating chondrocyte and BMSC migration and infiltration. Additionally, BMSCs-EVs hydrogel possessed the most superior chemotactic impact on chondrocytes and BMSCs than other groups.

EVs-SIS hydrogel enhanced cartilage regeneration in vivo

The rat articular cartilage defect model was established to investigate whether EVs-SIS hydrogel can enhance vivo cartilage regeneration (Figure 6(a)). The macroscopic observation of cartilage regeneration at 10 weeks after surgery are shown in Figure 6(b). The repaired tissue was visible at the defect site in all groups, but the blank group and SIS hydrogel group contained large amounts of fibrous tissue-like tissue with an irregular surface and distinct borders between the newly formed tissue and the surrounding normal cartilage. The blank group has a rougher surface compared with SIS hydrogel group. In the SIS+NIH/3T3-EVs group and SIS+C20A4-EVs group, the defect regions were partially covered by white cartilage-like regenerated tissue, and the boundary was still obvious. The cartilage defects of the SIS+C28I2-EVs group and SIS+BMSCs-EVs group exhibited smooth and intact regenerated surfaces, completely filled with white cartilage-like regenerated tissue and had no obvious integrated borders, which was significantly better than the effect in the other four groups.

As for the histological evaluation, HE, toluidine blue, and Safranin O-fast green staining were used to illustrate the nature of regenerated tissue (Figure 6(c–e)). Firstly, SIS hydrogel structure was not observable in any group, demonstrating that the gel could be degraded in vivo within 10 weeks. The defect was filled with fibrous tissue in the blank group, and no characteristic chondrocyte phenotype or specific staining was observed. Other experiment groups showed cartilage-like regenerated tissues, but there were differences in new formation area, cell phenotype, and cartilage or subchondral bone structure. TB staining was used to calculate the new cartilage formation area, the SIS hydrogel group had the least area and the SIS+BMSCs-EVs group showed the most significant specific staining with the most mature chondrocyte phenotype (Figure 6(d)). The new-formed chondrocytes in the SIS+BMSCs-EVs group were caught in ovoid cartilage traps and surrounded by cartilage matrix. By 10 weeks, the cartilage formation ratio at the defect in the SIS+BMSCs-EVs group was nearly 70% (Figure 6(g)) with a Wakitani's histological score of 2.96 shown in Figure 6(f). The SIS+BMSCs-EVs group showed predominately hyaline cartilage formation characterized by high expression of COL II and ACAN, but low expression of COL I compared to other groups. In contrast, the blank group (PBS-treated) showed mostly fibrous tissue that stained more intensely and diffusely for COL I (Figure 7). The results showed that the SIS hydrogel promoted in situ cartilage regeneration, and this enhancement was more significant after EV modification, with the SIS+BMSCs-EVs hydrogel being the most effective for cartilage regeneration.

Proteomic profiling of fibroblast-EVs, chondrocyte-EVs, and BMSCs-EVs

Abundant proteins encapsulated in EVs are likely to perform vital functions in cell communication. To investigate the potential molecular mechanisms underlying EVs origin on cartilage regeneration, we evaluated the relative proteins abundance of NIH/3T3-EVs, C20A4-EVs, C28I2-EVs, and BMSCs-EVs using 4D label-free technology-based quantitative proteomics.

A detailed proteomic analysis of the different origins EVs identified 291, 626, and 543 proteins in fibroblasts-EVs, chondrocyte-EVs, and BMSC-EVs, respectively (Figure 8(a)), indicating that EV cargos are affected by the origin of specific tissues.

Gene ontology (GO) analysis revealed that EVs derived from distinct sources differentially enriched in biological process (BP), cellular component (CC), and molecular function (MF) (Figure 8(b–d)). In the top 20 enriched GO terms, BMSCs-EVs enriched 13 BP terms, more than fibroblast-EVs and chondrocyte-EVs, suggesting that BMSC-originated EVs are more likely to affect cell biological functions. Interestingly, among the multiple enriched biological process, BMSCs-EVs appeared to be mainly involved in the metabolic process, including the organic substance metabolic process, the cellular macromolecule metabolic process, the primary metabolic process, the macromolecule metabolic process, the nitrogen compound metabolic process, the cellular metabolic process, etc. (Figure 8(d, e)). In terms of cellular component, the identified proteins of BMSCs-EVs were significantly enriched in the cytoplasm region and ribonucleoprotein complex, while fibroblast-EVs and chondrocyte-EVs only enriched in the extracellular region and cytoplasm region (Figure 8(b–d)). The KEGG pathway analysis showed that, unlike fibroblast-EVs and chondrocyte-EVs, BMSCs-EVs proteins were mainly enriched in the ribosome pathway (Figure 8(f–h)).

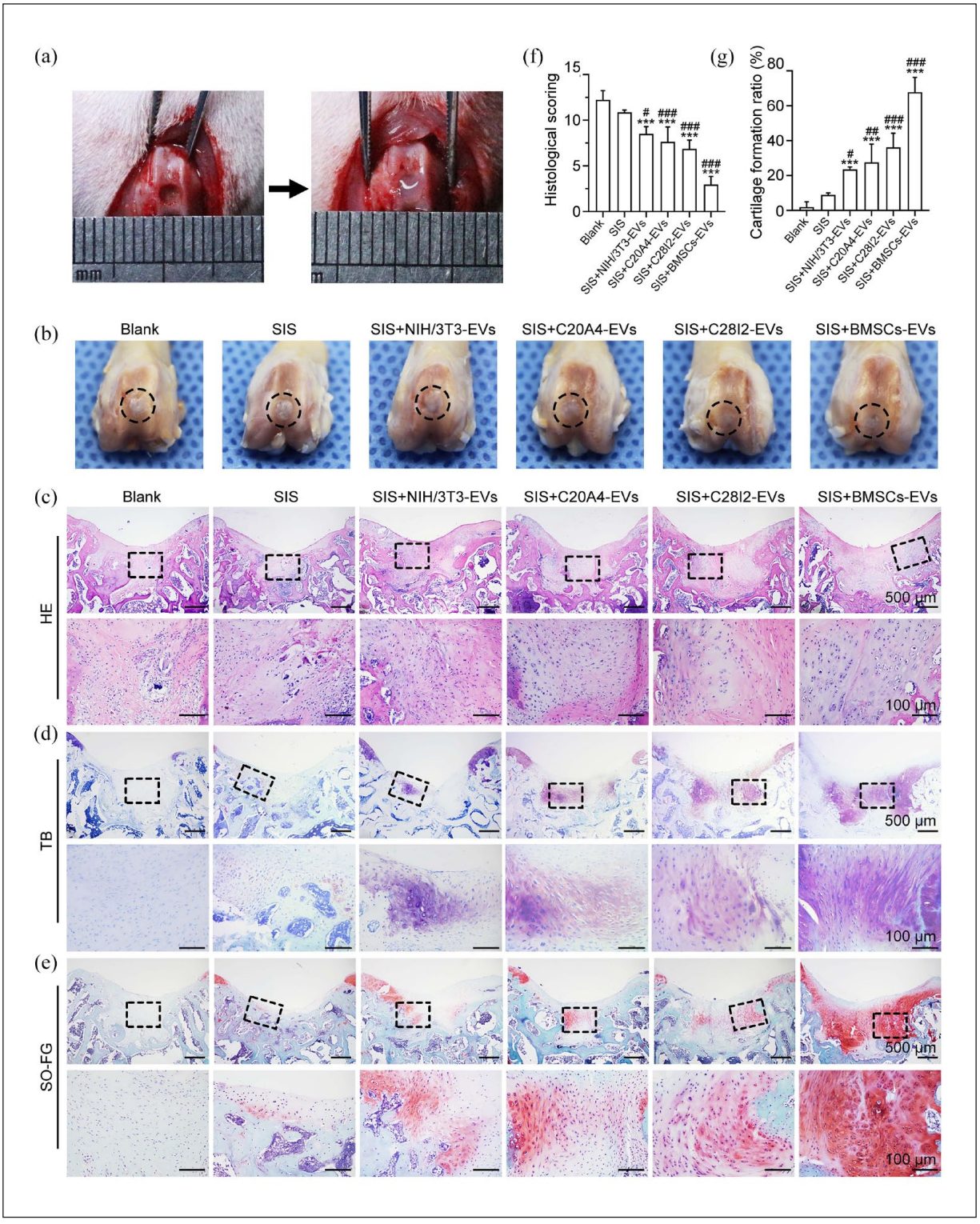

Figure 6. Macroscopic observation and histological evaluation of repaired tissue at 10 weeks after surgery: (a) the procedure of creating superficial articular cartilage defect model in patellar grooves and injecting hydrogel into the defect, (b) gross appearance of the repaired cartilage defects in the six groups, the dotted circles indicate the defect areas, (c–e) histological staining of repaired cartilage including hematoxylin and eosin staining (c), toluidine blue staining (d), and Safranin O/Fast Green staining (e), the rectangles indicate the areas shown in the under column at higher magnification, (f) histological scoring for the repaired tissues in different groups, (g) cartilage formation ratio was measured based on TB staining of defects cross-sections.
*Compared with blank group. #Compared with SIS+BMSCs-EVs group. */#$p < 0.05$. **/##$p < 0.01$. ***/###$p < 0.001$. $n = 5$ (five sections were measured for each rat and five rats were analyzed for each group).

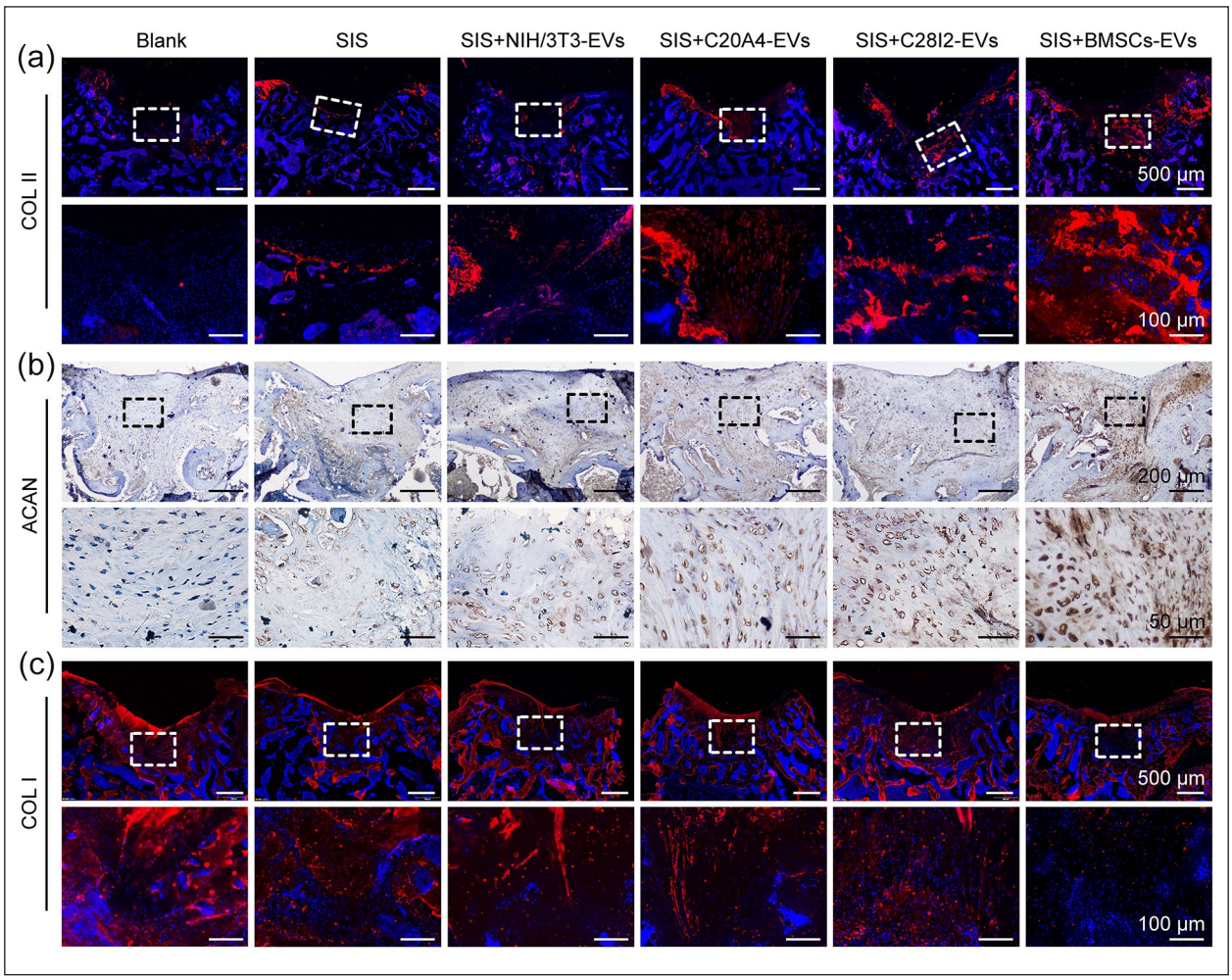

Figure 7. Expression of extracellular matrix proteins in the cartilage defect at 10 weeks after surgery: (a) immunofluorescence staining for COL II, (b) immunohistochemical staining for ACAN, (c) immunofluorescence staining for COL I.
The rectangles indicate the areas shown in the under column at higher magnification.

Moreover, a comparison of the protein abundance range confirmed that BMSCs-EVs is enriched in metabolic process and ribosome pathway. Though the total protein number of BMSCs-EVs in cellular macromolecular metabolic processes term is less than that of C20A4-EVs and C28I2-EVs, the associated proteins had higher abundance, with 25 associated proteins ranked in the top 50 and 58 in the top 200 (Figure 9(a–e)). For the ribosome pathway, NIH/3T3-EVs, C20A4-EVs, and C28I2-EVs are all enriched for only two proteins, while BMSCs-EVs had a greater number of associated proteins with higher abundance, indicating that BMSCs-EVs is associated with ribosome composition and further affect cellular biosynthesis (Figure 9(a–d)). As expected, BMSCs-EVs specifically upregulated multiple biosynthetic GO terms compared to the other three sources of EVs, which may be associated with the superior ability in vivo and in vitro cartilage regeneration (Figure 9(f)). The differential proteins were mainly located in the cytoplasm, followed by the nuclear (Figure 9(g–i)).

Discussion

In the present study, we constructed SIS hydrogel delivery systems containing four different types of EVs as cartilage regenerative potential scaffolds. Chondrocytes and BMSCs play an indelible role in cartilage remodeling. Chondrocytes and the matrix they secrete directly form cartilage, but chondrocytes around the injured area typically have diminished vitality. BMSCs are fundamental cellular components during the cartilage regeneration processes. However, they present in very small amounts in the total bone marrow cell population (0.001–0.01%).[17] Also, the lack of vascular in cartilage prevents BMSCs from accessing the defect site. Therefore, the capability of chondrocytes and BMSCs to

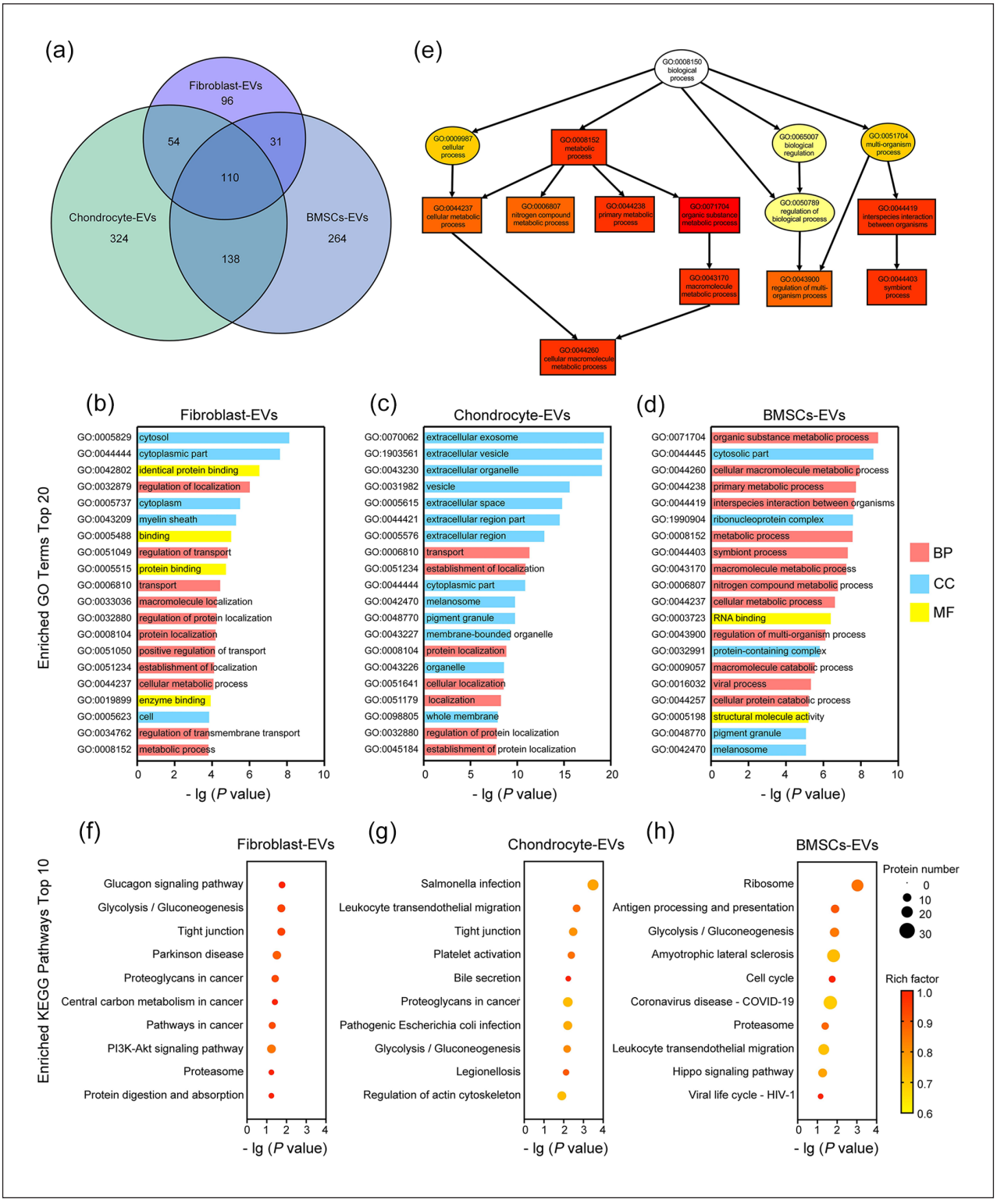

Figure 8. Quantitative proteomic analysis of EVs from different origins: (a) venn diagram of protein number from three origins EVs, (b–d) GO analysis for the top 20 upregulated terms among different EVs, (e) directed acyclic graph (DAG) of the enriched GO terms. The ID and description of the GO term were presented, the branch represented the containment relationship, the color depth represented the degree of enrichment (red meant more significant), the rectangles represented the top 10 enriched GO terms, and the ellipses represented the remaining terms, (f–h) KEGG enrichment analysis for the upregulated pathways, the size of bubbles represented the protein number involved, and the color represented the rich factor. ($n = 3$).

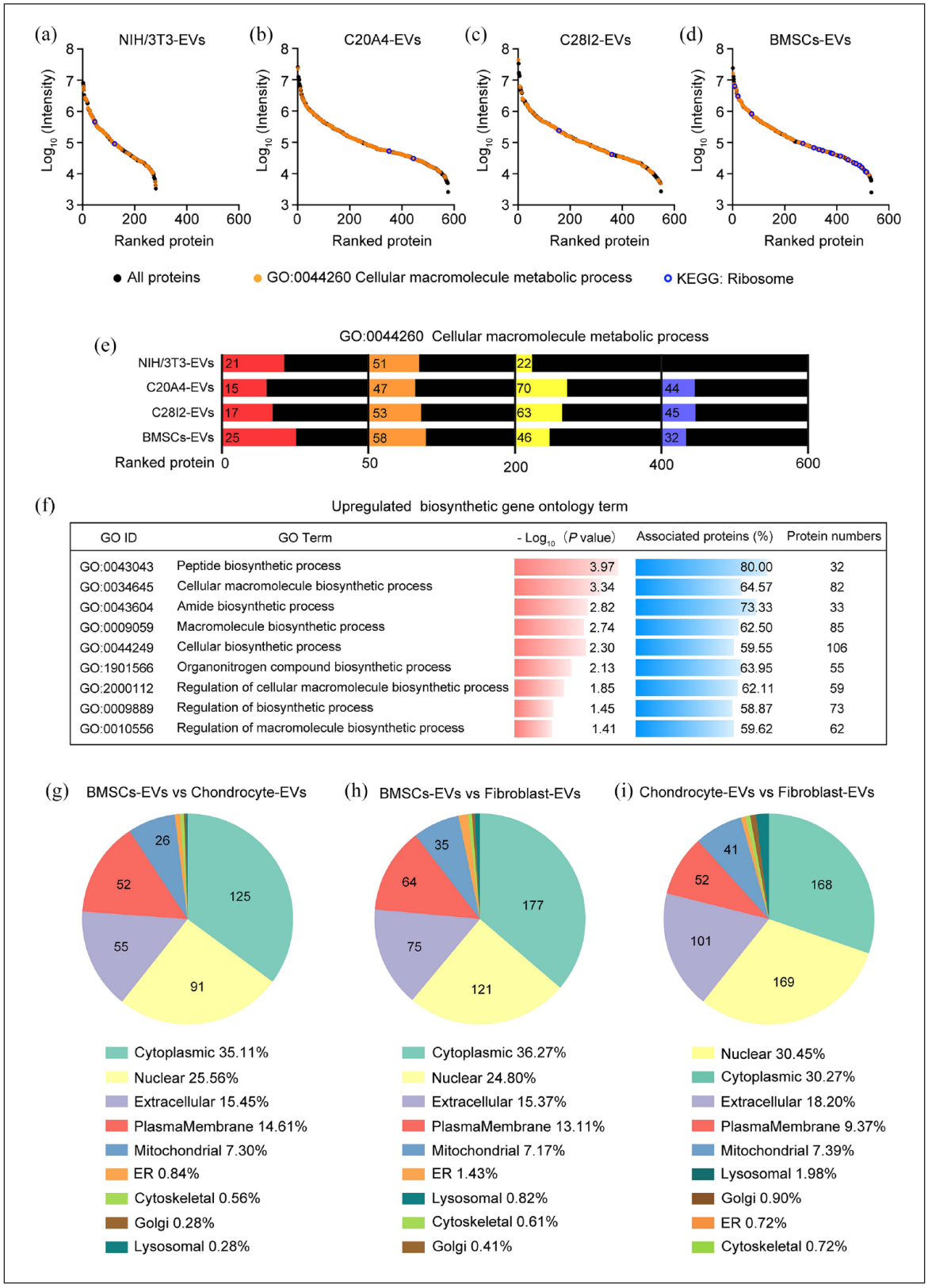

Figure 9. Proteomic analysis reveals a potential mechanism for BMSCs-EVs superiority in cartilage regeneration: (a–d) protein abundance range, proteins mapped to GO-BP:0044260 highlighted to the orange-dot, blue-circles represented the proteins mapped to KEGG: ribosome pathway, (e) the abundance distribution of proteins involved in GO-BP:0044260, (f) table of GO terms enriched in BMSCs-EVs involved in biosynthetic, (g–h) the cytolocalization of differential proteins for BMSCs-EVs versus chondrocyte-EVs, BMSCs-EVs versus fibroblast-EVs, and fibroblast-EVs versus chondrocyte-EVs.

keep viability, migrate into defects, and undergo chondrogenic differentiation is crucial for successful cartilage regeneration. Cumulative evidence has shown that complex local heterogeneous microenvironments modulate cell biology via cell-matrix interactions by activating intracellular signaling cascades.[38,39] Thus, providing chondrocytes and BMSCs in injury situ with a potential chondrogenesis microenvironment is a primary objective of cartilage tissue engineering.

Consistent with some research focused on single type EVs, all four origins EVs investigated in our experiments contribute to the construction of the chondrogenesis microenvironment, and further facilitate cartilage regeneration. However, they have distinct cartilage therapeutic efficiency. From the perspective of the chondrogenesis timeline, we found that the capability of EVs to promote cell proliferation and migration diminished as BMSCs chondrogenic differentiation into chondrocytes, but the capability to promote chondrogenic differentiation was generally maintained and shown to be strongest in the adult chondrocyte. Notably, EVs originated from earlier chondrogenesis stages (BMSCs-EVs) have the optimal overall ability within the three stages, which showed several distinguished signatures: (1) Produce high yields of EVs (Figure 1(c)): Although slightly lower than fibroblasts, they are significantly higher than juvenile chondrocytes (4.3-fold) and adult chondrocytes (3.9-fold), which could better avoid the limitation of clinical application by the inefficiency of the EVs expansion system; (2) High uptake efficiency (Figure 1(c)); (3) Effective regulation of proliferation (Figure 2(a–d)), migration (Figure 3; 2(l–m)) and chondrogenic differentiation (Figure 2(e–j)) in vitro: optimal proliferation and migration ability, and second only to adult chondrocytes-EVs in chondrogenic differentiation; (4) Far superior in vivo cartilage regeneration efficiency. Previous studies have found that BMSC-EVs and chondrocyte-EVs could influence cartilage remodeling in their own ways. BMSCs-EVs could affect cell fate and regulate physiological /pathological processes during cartilage remodeling, including restoring mitochondrial function in degenerative chondrocytes,[40] recruiting BMSCs via the chemokine signaling pathways,[16] or modulating the biological phenotypes of OA-related cells.[41] Also, normal chondrocyte-secreted EVs could facilitate chondrogenic differentiation, promote matrix biosynthesis,[42] restore mitochondrial dysfunction, and enhance macrophage M2 polarization.[15] BMSCs-EVs also have a positive effect on the other resident cellular within the joint space. Uptake by fibroblast-like synoviocytes (FLS)[43,44] and synovial macrophage,[45] BMSCs-EVs can release cartilage damage and rheumatoid arthritis (RA). However, osteoarthritis (OA) chondrocyte-EVs play the opposite role in cartilage regeneration.[46] Overall, advanced than previous studies, we revealed BMSC-EVs showed higher bioactivity of chondrogenesis than chondrocytes-EVs and Fibroblasts-EVs, while juvenile chondrocyte-EVs and adult chondrocyte-EVs showed comparable effects.

The regulation of cellular genes and proteins during chondrogenesis may contribute to the differences between their corresponding EVs. BMSCs-EVs showed superior chondrogenesis ability probably due to the unique regenerative and renewal characteristic of stem cells. Chondrocytes-EVs exhibit significant chondrogenic differentiation effects possibly because they contain direct cartilage-oriented signals during the middle to mature chondrogenesis stages. Huynh et al.[47] revealed the temporal gene signature of BMSCs during chondrogenesis through transcriptomic profiling, they indicated a very high abundance of genes modulated during early chondrogenic differentiation. Cellular proliferation (DNA replication, nucleosome assembly, chromosome, cell cycle) was highly up-regulated during the early stage (d1–d3) and subsequently down-regulated at later time points, while occurring concurrently with chondrogenic markers (COL2A1, ACAN, COL9A1, COL11A1, COMP) significantly up-regulated, suggesting a switch from a proliferative to chondrogenic differentiation. They also found the cells at terminal chondrogenesis stage (d21) showed increased hypertrophic and fibroblastic markers both at gene level (COL10A1, MMP13, COL1A1) and protein level (COL I, COL X), signifying the potential of chondrogenically induced BMSCs to hypertrophic or fibroblastic phenotype at terminal stage.

Fibroblasts are abundant around cartilage tissue and accumulate in the early stages of osteochondral regeneration. Meanwhile, ECM secreted by fibroblasts have been shown to promote tissue regeneration including muscles, nerves, and vessels.[48] In this study, EVs from fibroblasts were successfully taken up by chondrocytes and BMSCs, further promoting their proliferation and migration, but they did not enhance chondrogenic differentiation or even inhibit it. It has become clear that resident synovial fibroblasts actively impel joint damage and inflammation. In recent years, investigators divided fibroblasts into distinct subsets with non-overlapping effector-cell functions, including cartilage destruction by producing MMPs and inducing osteoclastogenesis, and immuno-inflammatory regulation through producing inflammatory cytokines and chemokines.[49,50] These effects are likely to be induced by EVs.[51] Our results may indicate that stimulated fibroblasts secrete EVs recruit endogenous chondrocytes and BMSCs to the site and promote cell viability when injured. Nevertheless, fibroblast EVs are detrimental to stabilizing the cartilage phenotype. Some studies modified fibroblast EVs and successfully applied them to cartilage protection and regeneration.[21,52]

Though EVs have been recognized as functional bioactive agents with diverse biochemical components to modulate complex microenvironments and are widely used in tissue regeneration, the question remains why they work

specifically. Thus far, most research on EVs has concentrated on RNA molecules, although some studies have been conducted based on proteomics analysis.[11,53] They have not investigated and compared the EVs derived from cells at different chondrogenesis stages. Our proteomic analysis rationalizes the outstanding functionalities of EVs from the early chondrogenesis stage, mainly because they promote metabolic and synthetic processes. Evidence has demonstrated that pathological chondrocytes exhibit metabolic imbalances, including depletion of ATP and NADPH[54] and increased production of reactive oxygen species (ROS) and matrix metalloproteinases (MMPs).[55] The energy stress in pathological chondrocytes, coupled with a shift in metabolic pathways towards glycolysis, reduces energy expenditure in proliferation and protein synthesis processes, resulting in ECM protein synthesis and anabolism impairment, including collagen and proteoglycans.[56] Some experiments facilitated cartilage repair revolve around enhancing the metabolism process. Chen et al. developed plant-derived photosynthetic system using chondrocyte membranes to encapsulate nanothylakoid units, this system increased intracellular ATP and NADPH levels in situ, restored cellular metabolism, and protected against pathological progression of OA.[57] Our experiments confirm the proteins contained in BMSCs-EVs significantly upgrade multiple metabolic processes, which may provide a simple and efficient way to ameliorate cartilage regeneration caused by metabolism-induced cellular energy deficits. In addition, lipids (fatty acids and cholesterol) and amino acid metabolic abnormality are likely to be involved in OA pathogenesis and pathology.[58] The regulation of organic substance metabolic process by BMSCs-EVs may help to cope with OA-related cartilage degeneration. BMSCs-EVs enhanced the nitrogen compound metabolic process, which may be helpful for scavenging the complexes of ROS with reactive nitrogen species (RNS) produced by cartilage oxidative stress, reducing cytotoxicity.[59] All known organisms use ribosomes for protein synthesis. Consequently, BMSCs-EVs significantly enriched ribosomal pathway associates with upregulated multiple biosynthesis GO terms, promoting intracellular biosynthesis and extracellular matrix deposition. Moreover, our findings revealed that BMSCs-EVs express a high abundance of multiple proteins that have been shown to be beneficial for cartilage protection, including Mfge8 (ranked first),[60] Fn1 (ranked second),[61] Actg1 (ranked third),[62] Hspa8 (ranked sixth),[63] and Itgb1 (ranked 22nd).[64]

Hydrogels are ideal scaffolds for cartilage engineering,[65] dECM is widely used for tissue regeneration as they can facilitate a constructive and appropriate remodeling response in situ.[66,67] Considering that SIS has unique bioactivity and is broadly applied in reconstructive therapies,[68] we produced an injectable thermosensitive SIS ECM hydrogel as an EV delivery platform. According to DNA quantification results, almost all cellular components in the SIS dECM were removed (total quantified DNA of less than 50 ng/mg),[69] thereby preventing the dECM from eliciting an immune response (Figure 4(b)). Meanwhile, we preserved the maximum quantity of tissue-specific molecules such as collagen and GAGs, allowing the molecular composition of the scaffold more closely resemble cartilage natural matrix (Figure 4(c–d)). Our study demonstrated that SIS hydrogel has excellent biocompatibility and can promote the proliferation (Figure 5(d–e)) and migration (Figure 5(g–j)) of chondrocytes/BMSCs. We also focused on the applicability of different SIS concentration hydrogels used in cartilage tissue engineering and found that lower-concentration hydrogels are more readily infiltrated for cells (Figure 5(a–b)) but with low mechanical strength (Figure 4(h–i)), which may be based upon the greater interfiber distance (pore size) (Figure 4(e)). SEM results also revealed the biocompatibility, with the porous ultrastructure allows diffusion of nutrients and oxygen, which is essential to promote the chondrogenic phenotype.[70] Meanwhile, lower-concentration hydrogels gel more slowly and are less stable, increasing the difficulty of clinical application. Therefore, a medium-concentration hydrogel (8 mg/mL) is most suitable for cartilage tissue engineering.

Most importantly, SIS hydrogel can effectively load and release EVs. Each EVs-SIS hydrogel group showed apparently distinct chemotactic effects (Figure 5(l–o)), which is essentially consistent with the former EVs wound healing assay (Figure 3). The loose and porous 3D mesh structure is the structural basis for hydrogels to load EVs, and the appropriate porosity allows for effective loading and slow release.[71] The 3D encapsulation and tethering of ECM with EVs involves many interesting interactions. SIS hydrogel exists many positive charge groups,[72] which could react in an attractive manner with negatively charged phospholipid membranes of EVs to promote loading.[71] Adhesion molecules expressed on the surface of EVs, such as integrins, allow EVs to adhere to the ECM through the reaction between integrins and laminin and can be used to control the release of EVs from hydrogels.[73,74] Meanwhile, they present a special delivery pattern. dECM pre-gel with low modulus facilitates the distribution of EVs. The increased modulus of the hydrogel after gelation fixes the EVs in the cages. Subsequently, due to the high degree of cross-linking and the presence of surface channel proteins, ECM hydrogel deliver EVs internally and to neighborhood cells.[75] When cells proliferate and infiltrate into the hydrogel, they can also serve as channels for intercellular vesicle transport.[76] In the rat model, EVs-SIS hydrogel showed unique efficacy as a hydrogel delivery platform. Interestingly, SIS hydrogel without EVs also showed a trend of chondrogenic activity in vivo compared to the blank group, demonstrating the value of pure SIS hydrogel in cartilage regeneration applications.

Although we comprehensively compared the function and protein components of EVs from four cell origins, our

study has several limitations. OA and RA are both common inflammatory orthopedic diseases with a main pathological feature as cartilage degeneration, which are challenging to reverse through the existing medical technology. Therefore, further studies need to explore the effects of different EVs on cellular inflammatory activation, macrophage polarization, and the release of various proinflammatory mediators. Future research that integrates proteomics with microRNA differences and identifies critical differentially expressed genes/proteins could aid in the comprehension of the impact of EVs tissue origin differences on cartilage regenerative efficiency. The modification of EVs and SIS hydrogels to endow scaffolds with higher bioactivity and mechanical strength is the next research orientation.

Conclusion

In conclusion, we compared the chondrogenesis capacities of EVs derived from cells at different chondrogenesis stages and joined fibroblast-EVs. In vitro and in vivo results suggest the different cellular origin of EVs is a key factor influencing cartilage therapeutic efficiency. Although all four types of EVs are good candidates to facilitate cartilage regeneration, BMSC-EVs appear to be the best, then chondrocytes-EVs and fibroblast-EVs in sequence. The juvenile chondrocytes-EVs and adult chondrocytes-EVs showed comparable effect. These results indicate bone tissue-originated EVs are more effective than fibroblast-originated, while EVs derived from early chondrogenesis stage have better chondrogenesis capability. Proteomics analysis revealed that BMSCs-EVs specifically upregulated multiple metabolic and biosynthetic processes, which might be the potential mechanism. We also prepared injectable thermosensitive SIS hydrogel as an EV delivery platform for minimally invasive therapy. BMSCs-EVs+ SIS hydrogel showed better therapeutic effects in the rat articular cartilage defect model. Our study provided orientations for selecting EVs and suggested a feasible way to deliver EVs achieving long-term effects, which can be a promising strategy for cartilage regeneration.

Acknowledgements

The graphic abstract was created with BioRender.com.

Data availability

Data will be made available on request.

CRediT authorship contribution statement

Weilai Zhu: Data curation, Formal analysis, Investigation, Methodology, Software, Writing—original draft. Jiaying Shi: Formal analysis, Investigation. Bowen Weng: Investigation, Methodology. Zhenger Zhou: Formal analysis, Investigation. Xufeng Mao: Investigation. Senhao Pan: Investigation. Jing Peng: Formal analysis. Chi Zhang: Formal analysis. Haijiao Mao: Formal analysis, Funding acquisition. Mei Li: Conceptualization, Formal analysis, Funding acquisition, Resources, Validation, Writing—review & editing. Jiyuan Zhao: Conceptualization, Formal analysis, Funding acquisition, Resources, Supervision, Writing—review & editing.

Declaration of conflicting interests

The author(s) declared no potential conflicts of interest with respect to the research, authorship, and/or publication of this article.

Funding

The author(s) disclosed receipt of the following financial support for the research, authorship, and/or publication of this article: This work was supported by Natural Science Foundation of Zhejiang Province (LY22H060005, LBY23H180002); Natural Science Foundation of Ningbo(2021J003); Ningbo Public Welfare Science and Technology Foundation (2021S090); Ningbo Major Science and Technology Project (2024Z205, 2022Z133), and K. C. Wong Magna Fund in Ningbo University.

ORCID iD

Jiyuan Zhao https://orcid.org/0000-0002-1327-7119

References

1. Krishnan Y and Grodzinsky AJ. Cartilage diseases. *Matrix Biol* 2018; 71–72: 51–69.
2. Huey DJ, Hu JC and Athanasiou KA. Unlike bone, cartilage regeneration remains elusive. *Science* 2012; 338(6109): 917–921.
3. Basad E, Ishaque B, Bachmann G, et al. Matrix-induced autologous chondrocyte implantation versus microfracture in the treatment of cartilage defects of the knee: a 2-year randomised study. *Knee Surg Sports Traumatol Arthrosc* 2010; 18(4): 519–27.
4. Nie X, Chuah YJ, Zhu W, et al. Decellularized tissue engineered hyaline cartilage graft for articular cartilage repair. *Biomaterials* 2020; 235: 119821.
5. Makris EA, Gomoll AH, Malizos KN, et al. Repair and tissue engineering techniques for articular cartilage. *Nat Rev Rheumatol* 2015; 11(1): 21–34.
6. Hussey GS, Dziki JL and Badylak SF. Extracellular matrix-based materials for regenerative medicine. *Nat Rev Mater* 2018; 3(7): 159–173.
7. Mathieu M, Martin-Jaular L, Lavieu G, et al. Specificities of secretion and uptake of exosomes and other extracellular vesicles for cell-to-cell communication. *Nat Cell Biol* 2019; 21(1): 9–17.
8. Wang Y, Li S, Hu M, et al. Universal STING mimic boosts antitumour immunity via preferential activation of tumour control signalling pathways. *Nat Nanotechnol* 2024; 19(6): 856–866.
9. Zhang X, Song W, Liu Y, et al. Healthy tendon stem cell-derived exosomes promote tendon-to-bone healing of aged chronic rotator cuff tears by breaking the positive-feedback cross-talk between senescent tendon stem cells and macrophages through the modulation of macrophage polarization. *Small* 2024; 8: e2311033.
10. Li X, Li S, Fu X, et al. Apoptotic extracellular vesicles restore homeostasis of the articular microenvironment for the treatment of rheumatoid arthritis. *Bioact Mater* 2024; 35: 564–576.

11. Wang ZG, He ZY, Liang S, et al. Comprehensive proteomic analysis of exosomes derived from human bone marrow, adipose tissue, and umbilical cord mesenchymal stem cells. *Stem Cell Res Ther* 2020; 11(1): 511.
12. Baglio SR, Rooijers K, Koppers-Lalic D, et al. Human bone marrow- and adipose-mesenchymal stem cells secrete exosomes enriched in distinctive miRNA and tRNA species. *Stem Cell Res Ther* 2015; 6(1): 127.
13. Narayanan K, Kumar S, Padmanabhan P, et al. Lineage-specific exosomes could override extracellular matrix mediated human mesenchymal stem cell differentiation. *Biomaterials* 2018; 182: 312–322.
14. Kimiz-Gebologlu I and Oncel SS. Exosomes: large-scale production, isolation, drug loading efficiency, and biodistribution and uptake. *J Control Release* 2022; 347: 533–543.
15. Zheng L, Wang Y, Qiu P, et al. Primary chondrocyte exosomes mediate osteoarthritis progression by regulating mitochondrion and immune reactivity. *Nanomedicine (Lond)* 2019; 14(24): 3193–3212.
16. Zhang FX, Liu P, Ding W, et al. Injectable mussel-inspired highly adhesive hydrogel with exosomes for endogenous cell recruitment and cartilage defect regeneration. *Biomaterials* 2021; 278: 121169.
17. Pittenger MF, Mackay AM, Beck SC, et al. Multilineage potential of adult human mesenchymal stem cells. *Science* 1999; 284(5411): 143–147.
18. Danalache M, Umrath F, Riester R, et al. Proteolysis of the pericellular matrix: pinpointing the role and involvement of matrix metalloproteinases in early osteoarthritic remodeling. *Acta Biomater* 2024; 181: 297–307.
19. Kim M, Steinberg DR, Burdick JA, et al. Extracellular vesicles mediate improved functional outcomes in engineered cartilage produced from MSC/chondrocyte cocultures. *Proc Natl Acad Sci U S A* 2019; 116(5): 1569–1578.
20. Li M, Zhang A, Li J, et al. Osteoblast/fibroblast coculture derived bioactive ECM with unique matrisome profile facilitates bone regeneration. *Bioact Mater* 2020; 5(4): 938–948.
21. Lai C, Liao B, Peng S, et al. Synovial fibroblast-miR-214-3p-derived exosomes inhibit inflammation and degeneration of cartilage tissues of osteoarthritis rats. *Mol Cell Biochem* 2023; 478(3): 637–649.
22. Bei HP, Hung PM, Yeung HL, et al. Bone-a-petite: engineering exosomes towards bone, osteochondral, and cartilage repair. *Small* 2021; 17(50): e2101741.
23. Liu X, Inda ME, Lai Y, et al. Engineered living hydrogels. *Adv Mater* 2022; 34(26): e2201326.
24. Qian H, He L, Ye Z, et al. Decellularized matrix for repairing intervertebral disc degeneration: fabrication methods, applications and animal models. *Mater Today Bio* 2023; 18: 100523.
25. Wolf MT, Daly KA, Brennan-Pierce EP, et al. A hydrogel derived from decellularized dermal extracellular matrix. *Biomaterials* 2012; 33(29): 7028–7038.
26. Brown M, Li J, Moraes C, et al. Decellularized extracellular matrix: new promising and challenging biomaterials for regenerative medicine. *Biomaterials* 2022; 289: 121786.
27. Zhao Y, Peng H, Sun L, et al. The application of small intestinal submucosa in tissue regeneration. *Mater Today Bio* 2024; 26: 101032.
28. Giobbe GG, Crowley C, Luni C, et al. Extracellular matrix hydrogel derived from decellularized tissues enables endodermal organoid culture. *Nat Commun* 2019; 10(1): 5658.
29. Li M, Zhang C, Cheng M, et al. Small intestinal submucosa: a potential osteoconductive and osteoinductive biomaterial for bone tissue engineering. *Mater Sci Eng C Mater Biol Appl* 2017; 75: 149–156.
30. Li M, Gu Q, Chen M, et al. Controlled delivery of icariin on small intestine submucosa for bone tissue engineering. *Mater Sci Eng C Mater Biol Appl* 2017; 71: 260–267.
31. Li M, Zhang C, Mao Y, et al. A cell-engineered small intestinal submucosa-based bone mimetic construct for bone regeneration. *Tissue Eng Part A* 2018; 24(13–14): 1099–1111.
32. Kremer A, Ribitsch I, Reboredo J, et al. Three-dimensional coculture of meniscal cells and mesenchymal stem cells in collagen type I hydrogel on a small intestinal matrix-A pilot study toward equine meniscus tissue engineering. *Tissue Eng Part A* 2017; 23(9–10): 390–402.
33. Soleimani M and Nadri S. A protocol for isolation and culture of mesenchymal stem cells from mouse bone marrow. *Nat Protoc* 2009; 4(1): 102–106.
34. Simonsen JB. Pitfalls associated with lipophilic fluorophore staining of extracellular vesicles for uptake studies. *J Extracell Vesicles* 2019; 8(1): 1582237.
35. Chen C, Cai N, Niu Q, et al. Quantitative assessment of lipophilic membrane dye-based labelling of extracellular vesicles by nano-flow cytometry. *J Extracell Vesicles* 2023; 12(8): e12351.
36. Zhu Y, Kong L, Farhadi F, et al. An injectable continuous stratified structurally and functionally biomimetic construct for enhancing osteochondral regeneration. *Biomaterials* 2019; 192: 149–158.
37. Wiśniewski JR, Zougman A, Nagaraj N, et al. Universal sample preparation method for proteome analysis. *Nat Methods* 2009; 6(5): 359–362.
38. Uroz M, Wistorf S, Serra-Picamal X, et al. Regulation of cell cycle progression by cell-cell and cell-matrix forces. *Nat Cell Biol* 2018; 20(6): 646–654.
39. Johnston LA. Competitive interactions between cells: death, growth, and geography. *Science* 2009; 324(5935): 1679–1682.
40. Chen P, Zheng L, Wang Y, et al. Desktop-stereolithography 3D printing of a radially oriented extracellular matrix/mesenchymal stem cell exosome bioink for osteochondral defect regeneration. *Theranostics* 2019; 9(9): 2439–2459.
41. Ni Z, Zhou S, Li S, et al. Exosomes: roles and therapeutic potential in osteoarthritis. *Bone Res* 2020; 8: 25.
42. Mao G, Hu S, Zhang Z, et al. Exosomal miR-95-5p regulates chondrogenesis and cartilage degradation via histone deacetylase 2/8. *J Cell Mol Med* 2018; 22(11): 5354–5366.
43. Li GQ, Fang YX, Liu Y, et al. MicroRNA-21 from bone marrow mesenchymal stem cell-derived extracellular vesicles targets TET1 to suppress KLF4 and alleviate rheumatoid arthritis. *Ther Adv Chronic Dis* 2021; 12: 20406223211007369.
44. Wu H, Zhou X, Wang X, et al. miR-34a in extracellular vesicles from bone marrow mesenchymal stem cells reduces rheumatoid arthritis inflammation via the cyclin I/ATM/ATR/p53 axis. *J Cell Mol Med* 2021; 25(4): 1896–1910.

45. Shen X, Qin J, Wei Z, et al. Bone marrow mesenchymal stem cell exosome-derived lncRNA TUC339 influences the progression of osteoarthritis by regulating synovial macrophage polarization and chondrocyte apoptosis. *Biomed Pharmacother* 2023; 167: 115488.
46. Li Z, Wang Y, Xiang S, et al. Chondrocytes-derived exosomal miR-8485 regulated the Wnt/beta-catenin pathways to promote chondrogenic differentiation of BMSCs. *Biochem Biophys Res Commun* 2020; 523(2): 506–513.
47. Huynh NPT, Zhang B and Guilak F. High-depth transcriptomic profiling reveals the temporal gene signature of human mesenchymal stem cells during chondrogenesis. *FASEB J* 2019; 33(1): 358–372.
48. Zhu M, Li W, Dong X, et al. In vivo engineered extracellular matrix scaffolds with instructive niches for oriented tissue regeneration. *Nat Commun* 2019; 10(1): 4620.
49. Mizoguchi F, Slowikowski K, Wei K, et al. Functionally distinct disease-associated fibroblast subsets in rheumatoid arthritis. *Nat Commun* 2018; 9(1): 789.
50. Croft AP, Campos J, Jansen K, et al. Distinct fibroblast subsets drive inflammation and damage in arthritis. *Nature* 2019; 570(7760): 246–251.
51. Zeng G, Deng G, Xiao S, et al. Fibroblast-like synoviocytes-derived exosomal PCGEM1 accelerates IL-1beta-induced apoptosis and cartilage matrix degradation by miR-142-5p/RUNX2 in chondrocytes. *Immunol Invest* 2022; 51(5): 1284–1301.
52. Zhou Y, Ming J, Li Y, et al. Exosomes derived from miR-126-3p-overexpressing synovial fibroblasts suppress chondrocyte inflammation and cartilage degradation in a rat model of osteoarthritis. *Cell Death Discov* 2021; 7(1): 37.
53. Li Q, Yu H, Sun M, et al. The tissue origin effect of extracellular vesicles on cartilage and bone regeneration. *Acta Biomater* 2021; 125: 253–266.
54. Vaillancourt F, Fahmi H, Shi Q, et al. 4-Hydroxynonenal induces apoptosis in human osteoarthritic chondrocytes: the protective role of glutathione-S-transferase. *Arthritis Res Ther* 2008; 10(5): R107.
55. Loeser RF, Collins JA and Diekman BO. Ageing and the pathogenesis of osteoarthritis. *Nat Rev Rheumatol* 2016; 12(7): 412–420.
56. Stegen S, Laperre K, Eelen G, et al. HIF-1alpha metabolically controls collagen synthesis and modification in chondrocytes. *Nature* 2019; 565(7740): 511–515.
57. Chen P, Liu X, Gu C, et al. A plant-derived natural photosynthetic system for improving cell anabolism. *Nature* 2022; 612(7940): 546–554.
58. Zheng L, Zhang Z, Sheng P, et al. The role of metabolism in chondrocyte dysfunction and the progression of osteoarthritis. *Ageing Res Rev* 2021; 66: 101249.
59. Zhong G, Yang X, Jiang X, et al. Dopamine-melanin nanoparticles scavenge reactive oxygen and nitrogen species and activate autophagy for osteoarthritis therapy. *Nanoscale* 2019; 11(24): 11605–11616.
60. Lu Y, Liu L, Pan J, et al. MFG-E8 regulated by miR-99b-5p protects against osteoarthritis by targeting chondrocyte senescence and macrophage reprogramming via the NF-kappaB pathway. *Cell Death Dis* 2021; 12(6): 533.
61. van Hoolwerff M, Rodríguez Ruiz A, Bouma M, et al. High-impact FN1 mutation decreases chondrogenic potential and affects cartilage deposition via decreased binding to collagen type II. *Sci Adv* 2021; 7(45): eabg8583.
62. Luo H, Yao L, Zhang Y, et al. Liquid chromatography-mass spectrometry-based quantitative proteomics analysis reveals chondroprotective effects of astragaloside IV in interleukin-1beta-induced SW1353 chondrocyte-like cells. *Biomed Pharmacother* 2017; 91: 796–802.
63. Zhang Z, Fan J, Becker KG, et al. Comparison of gene expression profile between human chondrons and chondrocytes: a cDNA microarray study. *Osteoarthritis Cartilage* 2006; 14(5): 449–459.
64. Song EK, Jeon J, Jang DG, et al. ITGBL1 modulates integrin activity to promote cartilage formation and protect against arthritis. *Sci Transl Med* 2018; 10(462): eaam7486.
65. Wei W, Ma Y, Yao X, et al. Advanced hydrogels for the repair of cartilage defects and regeneration. *Bioact Mater* 2021; 6(4): 998–1011.
66. Kim JW, Nam SA, Yi J, et al. Kidney decellularized extracellular matrix enhanced the vascularization and maturation of human kidney organoids. *Adv Sci (Weinh)* 2022; 9(15): e2103526.
67. Smoak MM, Hogan KJ, Grande-Allen KJ, et al. Bioinspired electrospun dECM scaffolds guide cell growth and control the formation of myotubes. *Sci Adv* 2021; 7(20): eabg4123.
68. Andrée B, Bär A, Haverich A, et al. Small intestinal submucosa segments as matrix for tissue engineering: review. *Tissue Eng Part B Rev* 2013; 19(4): 279–291.
69. Gilbert TW, Freund JM and Badylak SF. Quantification of DNA in biologic scaffold materials. *J Surg Res* 2009; 152(1): 135–139.
70. Herlofsen SR, Küchler AM, Melvik JE, et al. Chondrogenic differentiation of human bone marrow-derived mesenchymal stem cells in self-gelling alginate discs reveals novel chondrogenic signature gene clusters. *Tissue Eng Part A* 2011; 17(7–8): 1003–1013.
71. Ju Y, Hu Y, Yang P, et al. Extracellular vesicle-loaded hydrogels for tissue repair and regeneration. *Mater Today Bio* 2023; 18: 100522.
72. Wang W, Zhang X, Chao NN, et al. Preparation and characterization of pro-angiogenic gel derived from small intestinal submucosa. *Acta Biomater* 2016; 29: 135–148.
73. Chang AC, Uto K, Homma K, et al. Viscoelastically tunable substrates elucidate the interface-relaxation-dependent adhesion and assembly behaviors of epithelial cells. *Biomaterials* 2021; 274: 120861.
74. Huang CC, Kang M, Shirazi S, et al. 3D Encapsulation and tethering of functionally engineered extracellular vesicles to hydrogels. *Acta Biomater* 2021; 126: 199–210.
75. Lenzini S, Bargi R, Chung G, et al. Matrix mechanics and water permeation regulate extracellular vesicle transport. *Nat Nanotechnol* 2020; 15(3): 217–223.
76. Xing H, Zhang Z, Mao Q, et al. Injectable exosome-functionalized extracellular matrix hydrogel for metabolism balance and pyroptosis regulation in intervertebral disc degeneration. *J Nanobiotechnology* 2021; 19(1): 264.